Novel Localized Waves and their Interaction Solutions for a Dimensionally Reduced (2+1)-dimensional Boussinesq Equation from N-soliton Solutions

Dipankar Kumar (dks.bsmrstu@gmail.com)
Bangabandhu Sheikh Mujibur Rahman Science and Technology University https://orcid.org/0000-0003-2949-166X

Md. Nuruzzaman
Bangabandhu Sheikh Mujibur Rahman Science and Technology University

Gour Chandra Paul
University of Rajshahi

Ashabul Hoque
Bangabandhu Sheikh Mujibur Rahman Science and Technology University

Research Article

Keywords: Boussinesq equation, Hirota bilinear method, Long-wave limit approach, N-solitons, Localized waves, Interaction solutions.

Posted Date: July 14th, 2021

DOI: https://doi.org/10.21203/rs.3.rs-666725/v1

Version of Record: A version of this preprint was published at Nonlinear Dynamics on January 31st, 2022. See the published version at https://doi.org/10.1007/s11071-021-07077-9.

Novel Localized Waves and their Interaction Solutions for a Dimensionally Reduced (2+1)-dimensional Boussinesq Equation from *N*-soliton Solutions

Dipankar Kumar[1,*], Md. Nuruzzaman[1], Gour Chandra Paul[2,*], Ashabul Hoque[2]

[1]Department of Mathematics, Bangabandhu Sheikh Mujibur Rahman Science and Technology University, Gopalganj 8100, Bangladesh

[2]Department of Mathematics, University of Rajshahi, Rajshahi 6205, Bangladesh

Abstract

The Boussinesq equation (BqE) has been of considerable interest in coastal and ocean engineering models for simulating surface water waves in shallow seas and harbors, tsunami wave propagation, wave over-topping, inundation, and near-shore wave process in which nonlinearity and dispersion effects are taken into consideration. The study deals with the dynamics of localized waves and their interaction solutions to a dimensionally reduced (2+1)-dimensional BqE from *N*-soliton solutions with the use of Hirota's bilinear method (HBM). Taking the long-wave limit approach in coordination with some constraint parameters in the *N*-soliton solutions, the localized waves (i.e., soliton, breather, lump, and rogue waves) and their interaction solutions are constructed. The interaction solutions can be obtained among localized waves, such as (i) one breather or one lump from the two solitons, (ii) one stripe and one breather, and one stripe and one lump from the three solitons, and (iii) two stripes and one breather, one lump and one periodic breather, two stripes and one lump, two breathers, and two lumps from the four solitons. It is to be found that all interactions among the solitons are elastic. The energy, phase shift, shape, and propagation direction of these localized waves and their interaction solutions can be influenced and controlled by the involved constraint parameters. The dynamical characteristics of these localized waves and their interaction solutions are demonstrated through some 3D and density graphs. The outcomes achieved in this study can be used to illustrate the wave interaction phenomena in shallow water.

Keywords. Boussinesq equation; Hirota bilinear method; Long-wave limit approach; *N*-solitons; Localized waves; Interaction solutions.

[*]Corresponding author
Email addresses: dks.bsmrstu@gmail.com (D. Kumar); nafizmath95@gmail.com (M. Nurruzzaman); gcpaul@ru.ac.bd (G. C. Paul); ashabulh@yahoo.com (A. Hoque)

1. Introduction

The research of localized waves is one of the foremost topics in the areas of nonlinear science and mathematical physics. In nonlinear science, solitons, lumps, breathers, and rogue waves are localized waves, which are important objects in nonlinear physical systems [1]. Due to its importance in nonlinear science, researchers have paid deep attention to the exploration of these localized waves to a family of nonlinear evolution equations (NLEEs). Generally, solitary waves are localized waves that propagate at a constant speed without changing their shape [2]. Such a wave shape preserves its identity after pair-wise collisions, caused by a cancellation of nonlinear and dispersive effects in any nonlinear models [2]. With numerical simulations, Hirota [3] validated the preservation of soliton identities after pair-wise collisions. But the detailed analysis of the numerical results exposed the existence of some ripples after a collision meaning that the original identity is not completely recovered [4]. Therefore, it is directive to explore exact solutions of NLEEs admitting soliton solutions for proper scrutiny of collisions.

It is worth mentioning that John Scott Russell, in 1834, first observed a solitary wave travelling along a Scottish canal, and thereafter in 1965, Zabusky and Kruskal introduced the term “soliton” [5, 6]. However, on the other hand, lumps are rationally decaying solutions that are localized in all spatial directions, while breathers are partially localized breathing waves with a periodic structure in one certain direction [7]. A rogue wave is a special kind of rational solution that is localized both in spatial and temporal directions [8, 9]. The mechanism of rogue/freak waves can be regarded as the high amplitude waves generated by the interaction of solitons and breathers [1, 10]. The concept of rogue/ freak waves in the ocean was first proposed by Draper in 1965 [1]. The nonlinear localized waves mentioned above (solitons, lumps, breathers, and rogue waves) appear in several fields, such as oceanography, fluids, plasma physics, mathematical physics, optical fibers, nonlinear optics, cold atoms, Bose-

Einstein condensates, and so on [11-14]. These localized waves also illustrate various significant instances in nature via some of their related nonlinear models. Besides, interactions among different localized waves are also an interesting topic in nonlinear science [15]. Regarding the interest, researchers have focused on the exploration of some novel interaction solutions among four types of nonlinear localized waves to the NLEEs.

Nowadays, analytic solutions have a great contribution in the diverse field of nonlinear science and physics for interpreting the hidden mechanism via some relevant NLEEs. In order to interpret such underlying mechanism to their nonlinear models, several effective methods have been developed and performed sophistically due to the accessibility of symbolic computation software that make it possible to perform the intricate and tedious calculations. Some examples of the effective analytic methods are the inverse scattering transform [16], the Backlund transformation [17], the Darboux transformation [18], the Kudryashov method [19], the modified Kudryshov method [20, 21], the generalized Kudryashov method [22], the Jacobi elliptic function expansion method [23], the sine-Gordon expansion method [24], the extended sinh-Gordon expansion method [25-27], the $(G'/G, 1/G)$-expansion method [28], the auxiliary equation method [29], the new auxiliary equation method [22, 30], the variable separation method [31], the Riemann-Hilbert space approach [7, 32], the Painlevé analysis [33], the Consistent Riccati expansion method [34], and the HBM [3, 9, 35-38].

Among the aforementioned methods, researchers have proved that the HBM is widely popular due to its simplicity and directness, which is particularly useful to derive N-soliton solutions to any nonlinear integrable models. Recently, with the use of the long-wave limit approach in coordination with constraint parameters, the localized waves including solitons, lumps, breathers, rogue waves, and their interaction solutions from N-soliton solutions have been found through a variety of nonlinear models, which are mostly published in 2018-2020 [1, 10, 39-48]. Among the cited refs. [1, 10, 39-48], no significant studies have been found for

analyzing the wave propagation dynamics of the localized waves and their interaction structures in shallow water through some relevant models. Although, in the past, Wazwaz [49] mentioned that the study of wave propagation of long waves in shallow water has become a dynamic research field in nonlinear science. As in ref. Jawad *et al.* [50], the dynamics of wave propagation in shallow water are seen in lakes, rivers, ocean beaches and sea, and described by the BqE, which leads to

$$u_{tt} - u_{xx} - \beta(u^2)_{xx} - \gamma u_{xxxx} = 0. \tag{1}$$

The BqE was first introduced by Joseph Boussinesq in the 1870s for modeling the propagation of shallow water waves in multiple directions [51]. In this regard, the BqE contributes to a dominant role in explaining different physical aspects in the field of ocean engineering, fluid dynamics, and plasma physics dealing with a variety of wave phenomena. In ocean and coastal engineering, oceanographers and coastal engineers use the BqEs for simulating surface water waves in shallow seas and harbors, dune, ocean basin-scale tsunami propagation, wave over-topping, inundation, and near shore wave process modeling in which nonlinearities and dispersion are seen to be taken into consideration [52-57]. It is of interest to note here that the physical behaviors of any nonlinear models can be explored by analyzing their localized waves and interaction solutions. The Boussinesq (Bq) model is one of the ideal models for simulating wave propagation on ocean surfaces. To study the wave propagation dynamics on the ocean surfaces, we will construct the nonlinear localized waves and their interaction solutions to a new integrable Bq model. For this purpose, first, we consider the new integrable (3+1)-dimensional BqE [52], which leads to

$$u_{tt} - u_{xx} - \beta(u^2)_{xx} - \gamma u_{xxxx} + \frac{\alpha^2}{4}u_{yy} + \alpha u_{yt} + \delta u_{xz} = 0, \tag{2}$$

where $\alpha, \beta, \gamma, \delta$ are arbitrary constants, and u is an unknown function that depends on the spatial coordinates (x, y, z), and temporal coordinate t. Eq. (2) explains the propagation of gravity waves on the water surface [52]. Wazwaz and Kaur [52] proposed the extended form

of BqE specified by Eq. (2) to testify the integrability conditions via the Painlevé test. The authors constructed real and complex multiple soliton solutions via the simplified Hirota's method, and some novel solutions via the $exp(-\varphi(\eta))$-expansion method.

It is noteworthy to mention here that Eq. (2) can be converted into the standard fourth-order BqE given by Eq. (1) if we set each of α and δ equal to zero. On the other hand, if we put $\delta = 0$ in Eq. (2), then it reduces to the (2+1)-dimensional BqE, which is consistent with that of Wazwaz and Kaur [52]. It is convenient to reduce Eq. (2) from (3+1)-dimensions to (2+1)-dimensions by setting $z = 0$, $z = x$, and $z = y$. If we set $z = 0$ in Eq. (2), it is converted to the new integrable (2+1)-dimensional BqE, which can be found in Wazwaz and Kaur [52]. However, if we set $z = x$ and $\delta = 1$ to Eq. (2), it is converted to (2+1)-dimensional BqE, but the second-order linear dispersion term (u_{xx}) of the equation will disappear. Therefore, this paper is devoted to the study of dimensionally reduced (2+1)-dimensional BqE to construct the localized waves and their interaction solutions by setting $z = y$ in Eq. (2), which leads to

$$u_{tt} - u_{xx} - \beta(u^2)_{xx} - \gamma u_{xxxx} + \frac{\alpha^2}{4}u_{yy} + \alpha u_{yt} + \delta u_{xy} = 0. \quad (3)$$

It is remarkable to mention here that Eq. (3) must follow the integrability conditions. In the past, the dimensionally reduced form of the generalized Kadomtsev-Petviashvili (gKP) and Boiti-Leon-Manna-Pempinelli (BLMP) equations were solved by Liu *et al.* [48] and Wu *et al.* [10], respectively, where both the group of investigators constructed the localized waves and their interaction solutions from N-soliton solutions via the HBM in coordination with long-wave limit approach presented in Ablowitz and Satsuma [58]. For constructing the localized waves and their interaction wave solutions to the gKP and BLMP equations, Liu *et al.* [48] reduced the (3+1)-dimensional gKP equation dimensionally after substituting $z = x$, and Wu *et al.* [10] reduced the (3+1)-dimensional BLMP equation dimensionally after substituting $z = 0$ and $z = x$. To the best of the authors' knowledge, the localized waves and their novel interaction solutions have never been reported, so far, to the dimensionally reduced (2+1)-

dimensional BqE given by Eq. (3). Therefore, the key aim of the study is to construct nonlinear localized waves and their variety of interaction solutions among the localized waves to the dimensionally reduced (2+1)-dimensional Hirota bilinear form BqE from N-solitons solutions via the long-wave limit approach in conjunction with some constraint parameters. It is to be pointed out here that the long-wave limit approach in coordination with some constraint parameters is relatively different over the direct search positive quadratic function, hyperbolic function, trigonometric function, and their combinations, and the homoclinic test function approaches, which can be found in refs. [35-38].

The organization of the paper is as follows. Sec.§2 deals with the N-soliton solutions of the new integrable (3+1)-dimensional BqE and its dimensionally reduced (2+1)-dimensional BqE via the HBM. Sec.§3 presents nonlinear localized waves and their novel interaction solutions of the reduced (2+1)-dimensional BqE from N-soliton solutions taking the long-wave limit approach in coordination with some constraint parameters. Finally, the discussion of the obtained results and conclusion are placed in Sec.§4.

2. N-soliton solutions to the novel integrable (3+1)-dimensional BqE and its dimensionally reduced from

We use the following dependent variable transformation [52]:

$$u = \frac{6\gamma}{\beta}(\ln f)_{xx}, \tag{4}$$

where $f(x, y, z, t)$ is an unknown function of spatio-temporal coordinates $x, y, z,$ and t.

Eq. (2) under the transformation given by Eq. (4) is then transformed into the Hirota bilinear equation (HBE) as

$$\left(D_t^2 - D_x^2 - \gamma D_x^4 + \frac{1}{4}\alpha^2 D_y^2 + \alpha D_y D_t + \delta D_x D_z\right)(f.f) = 0. \tag{5}$$

In Eq. (5), D_x, D_y, D_z, and D_t stand for Hirota's bilinear differential operators (HBDOs) defined by (see Kumar *et al.* [38])

$$D_x^\alpha D_y^\beta D_z^\gamma D_t^\eta (f.g) = \left(\frac{\partial}{\partial x} - \frac{\partial}{\partial x'}\right)^\alpha \left(\frac{\partial}{\partial y} - \frac{\partial}{\partial y'}\right)^\beta \left(\frac{\partial}{\partial z} - \frac{\partial}{\partial z'}\right)^\gamma \left(\frac{\partial}{\partial t} - \frac{\partial}{\partial t'}\right)^\eta f(x, y, z, t) g(x', y', z', t')|_{x=x', y=y', z=z' t=t'}, \tag{6}$$

where $\alpha,\ \beta,\ \gamma,$ and η are non-negative integers.

By virtue of the definition of HBDO and its properties, Eq. (5) is turned into the following form:

$$f_{tt}f - f_t^2 - f_{xx}f + f_x^2 - \gamma(f_{xxxx}f - 4f_{xxx}f_x + 3f_{xx}^2) + \frac{1}{4}\alpha^2\left(f_{yy}f - f_y^2\right) + \alpha\left(ff_{yt} - f_yf_t\right) + \delta(f_{xz}f - f_xf_z) = 0. \quad (7)$$

Based on the simplified HBM and the transformation given by Eq. (4), N-soliton solutions are obtained from

$$f_i = 1 + \sum_{i=1}^{N} e^{\theta_i} + \sum_{i<j}^{N} a_{ij}\, e^{(\theta_i+\theta_j)} + \sum_{i<j<k}^{N} a_{ij}a_{ik}a_{jk}e^{(\theta_i+\theta_j+\theta_k)} + \cdots + \left(\prod_{i<j} a_{ij}\right)\left(e^{\sum_{i=1}^{N}\theta_i}\right), \quad (8)$$

where θ_i and a_{ij} stand for denoting the dispersion variables and generalized phase shifts, respectively, and are given by

$$\theta_i = a_ix + b_iy + c_iz + \left(-\frac{1}{2}\alpha b_i - \sqrt{\gamma a_i^4 - \delta a_ic_i + a_i^2}\right)t + \omega_i,\ i = 1, 2, \ldots, N, \text{ and}$$

$$a_{ij} = \frac{4\gamma a_i^3a_j - 6\gamma a_i^2a_j^2 + 4\gamma a_ia_j^3 - \delta a_ic_j - \delta a_jc_i - 2\sqrt{a_i\left(\gamma a_i^3 - \delta c_i + a_i\right)}\sqrt{a_j\left(\gamma a_j^3 - \delta c_j + a_j\right)} + 2a_ia_j}{4\gamma a_i^3a_j + 6\gamma a_i^2a_j^2 + 4\gamma a_ia_j^3 - \delta a_ic_j - \delta a_jc_i - 2\sqrt{a_i\left(\gamma a_i^3 - \delta c_i + a_i\right)}\sqrt{a_j\left(\gamma a_j^3 - \delta c_j + a_j\right)} + 2a_ia_j},\ i, j = 1, 2, \ldots, N, \quad (9)$$

where $a_i, b_i, c_i,$ and ω_i are arbitrary constants associated with the amplitude and phase of the ith-soliton. It is pertinent to mention that Wazwaz and Kaur [52] have recently constructed the multiple solitons for Eq. (1) by using the above expression. So, we will not repeat its physical importance.

Without loss of generality, $z = y$ can be set in Eq. (5). Then, Eq. (5) is converted to the following HBE:

$$\left(D_t^2 - D_x^2 - \gamma D_x^4 + \frac{\alpha^2}{4}D_y^2 + \alpha D_yD_t + \delta D_xD_y\right)(f.f) = 0. \quad (10)$$

Also, the functions for obtaining N-soliton solutions of Eq. (10), the dispersion variables (θ_i), and the generalized phase shifts $\left(a_{ij}\right)$ are changed, respectively, into

$$f_i = 1 + \sum_{i=1}^{N} e^{\theta_i} + \sum_{i<j}^{N} a_{ij}\, e^{(\theta_i+\theta_j)} + \sum_{i<j<k}^{N} a_{ij}a_{ik}a_{jk}e^{(\theta_i+\theta_j+\theta_k)} + \cdots + \left(\prod_{i<j} a_{ij}\right)\left(e^{\sum_{i=1}^{N}\theta_i}\right), \quad (11)$$

where $\theta_i = a_i x + b_i y - \left(\frac{1}{2}\alpha b_i + \sqrt{\gamma a_i^4 - \delta a_i b_i + a_i^2}\right) t + \omega_i$, $i = 1, 2, \ldots, N$, (12)

and

$$a_{ij} = \frac{4\gamma a_i^3 a_j - 6\gamma a_i^2 a_j^2 + 4\gamma a_i a_j^3 - \delta a_i b_j - \delta a_j b_i - 2\sqrt{a_i\left(\gamma a_i^3 - \delta b_i + a_i\right)}\sqrt{a_j\left(\gamma a_j^3 - \delta b_j + a_j\right)} + 2a_i a_j}{4\gamma a_i^3 a_j + 6\gamma a_i^2 a_j^2 + 4\gamma a_i a_j^3 - \delta a_i b_j - \delta a_j b_i - 2\sqrt{a_i\left(\gamma a_i^3 - \delta b_i + a_i\right)}\sqrt{a_j\left(\gamma a_j^3 - \delta b_j + a_j\right)} + 2a_i a_j}, \; i, j = 1, 2, \ldots, N. \quad (13)$$

Using Eq. (11) with the aid of Eqs. (12) and (13) in Eq. (4), one can obtain the following N-soliton solutions of Eq. (2):

$$u = \frac{6\gamma}{\beta}(\ln f_i)_{xx}, \; i = 1, 2, \ldots, N, \quad (14)$$

where $f_i(x, y, t)$ is a function involving spatial coordinates x, y, and temporal coordinate t.

Taking $N = 1$, $N = 2$, $N = 3$, and $N = 4$ to Eq. (14) along with Eqs. (11)-(13), one can acquire one-stripe, two-stripe, three-stripe, and four-stripe bright solitons, respectively, of Eq. (3). These bright solitons are displayed in **Figs. 1(a)-(d)** under the suitable selection of the constraint parameters as $a_1 = 1$, $a_2 = -1$, $a_3 = 2$, $a_4 = -2$, $b_1 = 1$, $b_2 = -1$, $b_3 = 2$, $b_4 = -2$, $\omega_1 = 0$, $\omega_2 = 0$, $\omega_3 = 0$, $\omega_4 = 0$, $\alpha = 1$, $\beta = 1$, $\gamma = 1$, $\delta = 1$, and $y = 0$. Furthermore, **Figs. 1(e)-(h)** exhibit the corresponding density views of **Figs. 1(a)-(d)**. It is realized visually from **Figs. 1(a)-(d)** and **Figs. 1(e)-(h)** that the N-soliton solutions remain unchanged in their height, width, and speed before $t < 0$ and after $t > 0$. During interactions, the solitons change only their phases. Therefore, the interactions among the N-solitons are elastic. Now, if we set $\beta = -1$ instead of $\beta = 1$ in the N-soliton solutions given by Eq. (14), the bright type N-solitons are changed into the dark types in the (x, t)-plane. It is to be mentioned here that the interactions of the dark solitons maintain the similar behaviors as that of the bright solitons.

3. Localized waves and their interaction solutions among N-soliton solutions

In this section, we will discuss localized waves and their interaction solutions in the case of two-stripe, three-stripe, and four-stripe solitons.

3.1 Interaction solutions between two-stripe solitons

Here, we discuss two cross-stripe solitons, parallel-stripe solitons, x-periodic breather, y-periodic breather, lump, and rogue wave solutions of Eq. (3). By taking $N = 2$ in Eq. (11), one can derive a function for two-soliton solutions given by

$$f_2 = 1 + e^{\theta_1} + e^{\theta_2} + a_{12}e^{\theta_1+\theta_2}, \tag{15}$$

where θ_i and a_{ij} are given by Eqs. (12) and (13), respectively. Substitution of Eq. (15) into Eq. (14), yields the two-soliton solutions of Eq. (3) as

$$u = \frac{6\gamma}{\beta}(\ln f_2)_{xx}. \tag{16}$$

Case I: Two cross-stripe and two parallel-stripe solitons

In order to determine the intersection solutions between two stripe solitons of Eq. (3), the constraint parameters a_i, b_i, and ω_i need to satisfy the following conditions for Eq. (16) along with Eq. (15):

$$a_i = p_i,\ b_i = q_i,\ (i = 1, 2), \tag{17}$$

where p_i and q_i are real constants, $p_i \neq 0$, and $q_1 \neq q_2$.

For cross-stripe solitons, the cross-product of p_1, p_2, q_1, and q_2 follows $(p_1q_2 - p_2q_1) \neq 0$. In order to construct the two cross-stripe solitons, we use $p_1 = 3$, $p_2 = -2$, $q_1 = 3$, $q_2 = 0$, $\omega_1 = 0$, $\omega_2 = 0$, $\alpha = 1$, $\beta = 1$, $\gamma = 1$, and $\delta = 1$ in Eq. (16). Eq. (16) then becomes

$$u = 6\left(\ln\left(1 + e^{3x+3y-\left(\frac{3}{2}+\sqrt{81}\right)t} + e^{-2x-\sqrt{20}\,t} + \left(\frac{89+6\sqrt{5}}{17+6\sqrt{5}}\right)e^{x+3y-\left(\frac{3}{2}+\sqrt{20}+\sqrt{81}\right)t}\right)\right)_{xx}. \tag{18}$$

The class of solutions given by Eq. (18) corresponds to the two cross-stripe solitons, which are displayed in **Figs. 2(a)-(c).** The illustrations are produced in the (x, y)-plane for $t = -5$, $t = 0$, $t = 5$, respectively**.** On the other hand, **Figs. 2(d)-(f)** illustrate the density views of **Figs. 2(a)-(c),** respectively. It can be perceived from **Figs. 2(a)-(c)** and **Figs. 2(d)-(f)** that two solitons intersect with each other in the (x, y)-plane. It is also observed from **Figs. 2(d)-(f)** that one soliton is perpendicular to the x-axis and propagates along the negative direction of the axis of

x, and another soliton crosses diagonally in the (x, y)-plane. However, they propagate independently keeping their original shapes and amplitudes unaltered. On the other hand, for parallel-stripe solitons, the values of p_1, p_2, q_1, and q_2 satisfy $(p_1 - p_2)(q_1 - q_2) \neq 0$, but $p_1 q_2 - p_2 q_1 = 0$. As per the mentioned rules, if we take $p_1 = 5$, $p_2 = -3$, $q_1 = -5$, $q_2 = 3$, $\omega_1 = 0$, $\omega_2 = 0$, $\alpha = 1$, $\beta = 1$, $\gamma = 1$, and $\delta = 1$ in Eq. (16), it yields

$$u = 6\left(\ln\left(1 + e^{5x-5y+\left(\frac{5}{2}-\sqrt{675}\right)t} + e^{-3x+3y-\left(\frac{3}{2}+\sqrt{99}\right)t} + \left(\frac{115+3\sqrt{33}}{25+3\sqrt{33}}\right)e^{2x-2y+\left(1-15\sqrt{3}-3\sqrt{11}\right)t}\right)\right)_{xx}. \quad (19)$$

The solution indicated by Eq. (19) represents the two parallel-stripe solitons. For $t < 0$, two parallel-stripe solitons are separated from each other, one with higher amplitude and another with lower amplitude. At $t = 0$, these two stripes overlap with one other. For $t > 0$, two parallel-stripe solitons are separated further, but the positions of the solitons are found to be reverse than that of the solitons presented for time $t < 0$. Thus, the solitons alter their positions at the mentioned times, but the amplitudes of the solitons remain unchanged during propagation. Due to the shake of brevity, the figures are not included here.

Case II: One x-periodic breather

To construct one x-periodic breather wave solutions of Eq. (3), the constraint parameters a_i, b_i, and ω_i need to satisfy the following conditions for Eq. (16) along with Eq. (15):

$$a_1 = a_2^* = Im_1,\ b_1 = p_1, b_2 = p_1,\ \omega_1 = \omega_2 = 0, \text{ and } m_1 \neq 0, p_1 \neq 0. \quad (20)$$

Here and henceforth '$*$' refers to the complex conjugate of a complex number, where $I^2 = -1$. If we substitute the values of the constraint parameters as $m_1 = 1,\ p_1 = \frac{1}{2}$, $\omega_1 = 0$, $\omega_2 = 0$, $\alpha = 1$, $\beta = 1$, $\gamma = 1$, and $\delta = 1$ into Eq. (16), it turns into the following form:

$$u = 6\left(\ln\left(1 + 2e^{\frac{1}{2}y-\frac{3}{4}t}\cos\left(x + \frac{1}{2}t\right) + 13\, e^{y-\frac{3}{2}t}\right)\right)_{xx}. \quad (21)$$

The solution specified by Eq. (21) presents one x-periodic breather wave, which is displayed in **Figs. 3(a)-(c)** at $t = -5$, $t = 0$, and $t = 5$, respectively. On the other hand, **Figs. 3(d)-(f)** illustrate the density views of **Figs. 3(a)-(c)** for a clear understanding. It can be realized from

Fig. 3 that with the evolution of time ($t = -5, 0, 5$), the positions of x-periodic breather are changed from the negative direction of the y-axis to its positive direction. However, the shape and amplitude of the x-periodic breather wave remain unchanged.

Case III: One xy-periodic breather

To find one xy-periodic breather wave solutions of Eq. (3), the constraint parameters a_i, b_i, and ω_i are prerequisite to satisfy the following conditions for Eq. (16) together with Eq. (15):

$$a_1 = a_2 = l_1, b_1 = b_2^* = p_1 + Iq_1, \ \omega_1 = \omega_2 = 0, \text{and } l_1 \neq 0, p_1 \neq 0, q_1 \neq 0. \quad (22)$$

If we take $l_1 = \frac{1}{3}$, $p_1 = \frac{1}{3}$, $q_1 = 1$, $\omega_1 = 0$, $\omega_2 = 0$, $\alpha = 1$, $\beta = 1$, $\gamma = 1$, and $\delta = 1$ in Eq. (16), it reduces to the following form:

$$u = 6\left(\ln\left(1 + e^{\left(\frac{1}{3}x + \left(\frac{1}{3} - i\right)y + \left(-\frac{1}{6} + \frac{1}{2}i + \sqrt{\frac{1}{81} + \frac{1}{3}i}\right)t\right)} + e^{\left(\frac{1}{3}x + \left(\frac{1}{3} + i\right)y + \left(-\frac{1}{6} - \frac{1}{2}i - \sqrt{\frac{1}{81} - \frac{1}{3}i}\right)t\right)} + \left(\frac{\sqrt{730}-1}{\sqrt{730}-7}\right) e^{\left(\frac{2}{3}x + \frac{2}{3}y + \left(-\frac{1}{3} + \sqrt{\frac{1}{81} + \frac{1}{3}i} - \sqrt{\frac{1}{81} - \frac{1}{3}i}\right)t\right)}\right)\right)_{xx}. \quad (23)$$

The solution specified by Eq. (23) characterizes one xy-periodic breather and is displayed in **Figs. 4(a)** and **4(c)**. It is interesting to mention here that one xy-periodic breather can be changed into one y-periodic breather when we consider $p_1 = 0$ and substitute it to the solution u given by Eq. (16). To ensure such behavior, one y-periodic breather is illustrated in **Figs. 4(b)** and **4(d)**.

Case IV: Lump soliton and rogue wave solutions

In 1979, Ablowitz and Satsuma proposed a method called "long wave limit method" [58]. With the assist of this method, the lump solitons can be obtained from N-soliton solutions after imposing some restrictions on parameters. In order to compute one lump solution of Eq. (3), setting constraint parameters as $b_1 = m_1 a_1$, $b_2 = m_2 a_2$, $a_1 = l_1 \varepsilon$, $a_2 = l_2 \varepsilon$, and $\omega_1 = \omega_2^* = \pi i$ to Eq. (15), the function f_2 can be rearranged as

$$f_2 = (\eta_1 \eta_2 + A_{12}) l_1 l_2 \varepsilon^2 + O(\varepsilon^3). \quad (24)$$

Taking the long-wave limit as $\varepsilon \to 0$ in Eq. (24) along with Eq. (16), the lump soliton of Eq. (3) can be expressed as follows:

$$u = \frac{6\gamma}{\beta}\left(\frac{2}{\eta_1\eta_2 + A_{12}} - \frac{(\eta_1+\eta_2)^2}{(\eta_1\eta_2 + A_{12})^2}\right), \tag{25}$$

where

$$A_{12} = \delta(m_1 + m_2) + 2\left(\sqrt{1 - m_1\delta}\,\sqrt{1 - m_2\delta}\right) - 2, \tag{26}$$

and

$$\eta_i = x + m_i\, y - \left(\frac{1}{2}m_i\alpha + \sqrt{1 + \gamma - m_i\delta}\right)\, t, i = 1, 2. \tag{27}$$

Now, setting the constraint parameters as $m_1 = m_2^* = p_1 + Iq_1 (q_1 \neq 0)$ to Eqs. (25)-(27), we find that the two-solitons will degenerate into one lump soliton. Taking $p_1 = 1$, $q_1 = 1$, $\alpha = 1$, $\beta = 1$, $\gamma = 1$, and $\delta = 1$ in Eqs. (25)-(27), one can explore one lump-soliton solution. The time evolution 3D plots of lump soliton are exhibited in **Figs. 5(a)-(c)** at $t = -5$, $t = 0$, and $t = 5$, respectively, whereas, **Figs. 5(d)-(f)** demonstrate the density views of **Figs. 5(a)-(c),** respectively. It is clearly seen from the figures that the lump has one peak and two troughs. It is also seen from the figures that peak and trough amplitudes of the lump soliton remain unchanged when time increases ($t = -5, 0, 5$). But the crest and trough positions of the lump soliton are changed during the propagation in the (x, y)-plane. It is pinpoint to mention here that the line rogue wave can be derived from Eq. (3) through the class of solutions given by Eq. (25), if we assume m_1 and m_2 as real constants. The mentioned line rogue wave is a rational solution with the process of growth and decay [39]. The constraints for localized waves and their interaction solutions between two-stripe solitons are summarized in **Table 1**.

Table 1. The nonlinear localized waves from two-soliton solutions

N-soliton	Types of the localized waves	Constraints
$N=2$	Two stripe solitons	$a_1=l_1, a_2=l_2,\ b_1=p_1,\ b_2=p_2,\ \omega_1=\omega_2=0$. Cross intersection: $(l_1p_2-l_2p_1)\neq 0$. Parallel intersection: $(l_1-l_2)(p_1-p_2)\neq 0$; but $l_1p_2-l_2p_1=0$.
	One x-periodic breather	$a_1=a_2^*=Im_1,\ b_1=p_1, b_2=p_1,\ \omega_1=\omega_2=0$, and $m_1\neq 0, p_1\neq 0$.
	One y-periodic breather	$a_1=a_2=l_1,\ b_1=b_2^*=Iq_1, \omega_1=\omega_2=0$, and $l_1\neq 0, q_1\neq 0$.
	One (x,y)-periodic breather	$a_1=\ a_2=l_1, b_1=b_2^*=p_1+Iq_1,\ \omega_1=\omega_2=0$, and $l_1\neq 0, p_1\neq 0, q_1\neq 0$.
	One lump soliton	$b_r=m_ra_r, a_r=l_r\varepsilon\ (r=1,2),\ m_1=m_2^*=p_1+Iq_1, \omega_1=\omega_2^*=I\pi$, and $\varepsilon\to 0$.

3.2 Interaction solutions among three-stripe solitons

The following subsections discuss the interaction solutions among three-stripe solitons to the BqE by their graphical illustrations. Interaction solutions among three-stripe solitons, viz. three cross-stripe solitons, two parallel-stripe solitons with other one stripe soliton, three parallel-stripe solitons, one stripe soliton and one periodic breather, and one stripe soliton and one lump soliton can be obtained from three soliton solutions. In order to get such interaction solutions among three-stripe solitons, setting $N=3$ to Eq. (11), one can obtain a function for three-soliton solutions given by

$$f_3=1+e^{\theta_1}+e^{\theta_2}+e^{\theta_3}+a_{12}e^{\theta_1+\theta_2}+a_{13}e^{\theta_1+\theta_3}+a_{23}e^{\theta_2+\theta_3}+a_{123}e^{\theta_1+\theta_2+\theta_3}, \quad (28)$$

where θ_i and a_{ij} are specified by Eqs. (12) and (13), respectively, and the phase shift satisfies the equation $a_{123}=a_{12}a_{23}a_{13}$. Now, plugging Eq. (28) into Eq. (14), the class of three-soliton solutions of Eq. (3) is found in the following form:

$$u=\frac{6\gamma}{\beta}(\ln f_3)_{xx}. \quad (29)$$

On restricting certain conditions on the specified parameters and a long-wave limit approach, one can construct several types of localized interaction solutions. Exploration of these solutions is described in detail as follows.

Case I: Interaction between two parallel stripe solitons and other one stripe soliton

Here, we would like to interact the two parallel stripe solitons with other one stripe soliton among three-stripe solitons of Eq. (3), the involved constraint parameters a_i, b_i, and ω_i require to maintain the following conditions for Eq. (29):

$$a_i = p_i,\ b_i = q_i,\ (i = 1, 2, 3), \text{ and } \omega_1 = \omega_2 = \omega_3 = 0, \tag{30}$$

where p_i, q_i are real constants, $\prod_{i\neq j}(p_i q_j - p_j q_i) = 0$, and $\sum_{i\neq j}(p_i q_j - p_j q_i)^2 \neq 0$.

Taking $p_1 = 3$, $p_2 = -2$, $p_3 = 1$, $q_1 = 3$, $q_2 = 2$, $q_3 = 1$, $\omega_1 = 0$, $\omega_2 = 0$, $\omega_3 = 0$, $\alpha = 1$, $\beta = 1$, $\gamma = 1$, and $\delta = 1$, one can obtain the interaction solution among two parallel stripe solitons and other one stripe soliton. The time evolution 3D plots of a solution from the class of solutions given by Eq. (29) for $t = -5$, $t = 2$, and $t = 5$ is displayed in **Figs. 6(a)-(c)**, whereas **Figs. 6(d)-(f)** display the respective density views of **Figs. 6(a)-(c)** for a better perspective. It is seen from Fig. 6 that the two parallel solitons merge at $t = 0$. But, two parallel solitons separate and intersect with the remaining one soliton normally at $t = -5$ as well as at $t = 5$. If the constraint parameters satisfy the condition $\prod_{i\neq j}(p_i q_j - p_j q_i) \neq 0$ for Eq. (28), the solution obtained from Eq. (29) represents three cross-stripe solitons. Alternatively, if the constraint parameters satisfy the condition $\sum_{i\neq j}(p_i q_j - p_j q_i)^2 = 0$ for Eq. (28), the class of solutions given by Eq. (29) represents three parallel-stripe solitons. Due to the sake of conciseness, three cross-stripe and three parallel-stripe solitons are not displayed here. For three cross-stripe solitons, the selected parameters are $p_1 = 3$, $p_2 = 2$, $p_3 = 1$, $q_1 = 3$, $q_2 = -2$, $q_3 = -0.5$, $\omega_1 = 0$, $\omega_2 = 0$, $\omega_3 = 0$, and $p_1 = 3$, $p_2 = 2$, $p_3 = 1$, $q_1 = 3$, $q_2 = 2$, $q_3 = 1$, $\omega_1 = 0$, $\omega_2 = 0$, $\omega_3 = 0$ are selected for three parallel-stripe solitons. For both cases, $\alpha = 1$, $\beta = 1$, $\gamma = 1$, and $\delta = 1$ are used.

Case II: One stripe soliton and one periodic breather

To consider the interaction solutions between one stripe soliton and one (x, y)-periodic breather wave for Eq. (3), the constraint parameters a_i, b_i, and ω_i allow to maintain the following conditions for Eq. (29):

$a_1 = l_1 + Im_1$, $a_2 = l_1 - Im_1$, $b_1 = p_1 + Iq_1$, $b_2 = p_1 - Iq_1$, $a_3 = l_2$, $b_3 = p_2$, and $\omega_1 = \omega_2 = \omega_3 = 0$, (31)

where $l_1 \neq 0$, $l_2 \neq 0$, $m_1 \neq 0$, $p_1 \neq 0$, $p_2 \neq 0$, and $q_1 \neq 0$.

It is mentionable at this juncture that for the parallel one stripe soliton and one (x, y)-periodic breather wave, the constraint parameters must follow the condition $l_1 p_2 - l_2 p_1 = 0$, and for the cross one stripe soliton and one (x, y)-periodic breather wave, the constraint parameters must satisfy the condition $l_1 p_2 - l_2 p_1 \neq 0$. Now, if we set the constraint parameters as $a_1 = a_2 = 0.25$, $a_3 = -0.75$, $b_1 = b_2^* = -0.25 + 0.75I$, $b_3 = 0.75$, $\omega_1 = 0$, $\omega_2 = 0$, $\omega_3 = 0$, $\alpha = 1$, $\beta = 1$, $\gamma = 1$, and $\delta = 1$ to Eq. (29), it corresponds to the interaction solution between the parallel one stripe soliton and one (x, y)-periodic breather wave. The time evolution density graphs of the respective solution at time $t = -5$, $t = 0$, and $t = 5$ are demonstrated through **Figs. 7(a1)-(a3)**. At time $t = -5$, one stripe soliton and one (x, y)-periodic breather waves are separated (see **Fig. 7(a1)**). Then, at time $t = 0$, they are merged together (see **Fig. 7(a2)**). Finally, at time $t = 5$, they are separated again. During the propagation, the amplitudes of the soliton and breather remain unchanged. The interaction behaviors of stripe and breather waves are elastic. It is worthy of note here that if we set $l_1 = 0$, $q_1 = 0$ to the condition given by Eq. (31), the interaction between one stripe soliton and one (x, y)-periodic breather reforms to the interaction between one stripe soliton and one x-periodic breather. By selecting the constraint parameters as $a_1 = a_2^* = 0.25I$, $a_3 = -0.75$, $b_1 = b_2 = -0.25$, $b_3 = 0.75$, $\omega_1 = 0$, $\omega_2 = 0$, $\omega_3 = 0$, $\alpha = 1$, $\beta = 1$, $\gamma = 1$, and $\delta = 1$ to the condition specified by Eq. (31), the time evolution density graphs of one stripe soliton and one x-periodic breather are presented in **Figs.**

7(b1)-(b3). It is perceived from **Figs. 7(b1)-(b3)** that the breather soliton is propagating parallelly along the x-axis. Furthermore, if we set $m_1 = 0, p_1 = 0$ to the condition given by Eq. (31), the collision between one stripe soliton and one (x, y)-periodic breather turns into the collision between one stripe soliton and one y-periodic breather. Setting the constraint parameters $a_1 = a_2 = 0.25$, $a_3 = -0.75$, $b_1 = b_2^* = 0.75I$, $b_3 = 0.75$, $\omega_1 = 0$, $\omega_2 = 0$, $\omega_3 = 0$, $\alpha = 1$, $\beta = 1$, $\gamma = 1$, and $\delta = 1$ to Eq. (29), one can produce the interaction solution between one stripe soliton and one y-periodic breather. The time evolution density graphs of one stripe soliton and one y-periodic breather are displayed in **Figs. 7(c1)-(c3).** In this case, the corresponding figures show that the breather wave propagates parallelly along the y-axis. It can be observed from each panel of density graphs that with the evolution of time, the stripe and all periodic breathers change their positions retaining their amplitudes unchanged.

Case III: One lump soliton and one stripe soliton

In order to detect the interaction solutions between one lump soliton and one stripe soliton for Eq. (3), the constraint parameters a_i, b_i, and ω_i require to maintain the following conditions for Eq. (29) in consort with Eq. (28):

$$b_1 = m_1 a_1,\ b_2 = m_2 a_2, b_3 = m_3 a_3, a_1 = l_1 \varepsilon, a_2 = l_2 \varepsilon, \omega_1 = \omega_2^* = I\pi, \text{ and } \omega_3 = 0. \tag{32}$$

Inserting the values presented in Eq. (32) into Eq. (28), it is possible to present the function f_3 as

$$f_3 = (A_{12} + \eta_1\eta_2)\, l_1 l_2 \varepsilon^2 + (\eta_1\eta_2 + A_{23}\eta_1 + A_{13}\eta_2 + A_{12} + A_{12}A_{23}) e^{\theta_3}\, l_1 l_2 \varepsilon^2 + O(\varepsilon^3). \tag{33}$$

Taking the long-wave limit as $\varepsilon \to 0$ in Eq. (33), the class of interaction solutions between one lump and one stripe soliton of Eq. (3) can be obtained from Eq. (29). This leads to

$$u = \frac{6\gamma}{\beta}\left(ln\left(\left(A_{12} + \eta_1\eta_2\right) + \left(\eta_1\eta_2 + A_{23}\eta_1 + A_{13}\eta_2 + A_{12} + A_{12}A_{23}\right)e^{\theta_3} \right) \right)_{xx}, \tag{34}$$

where

$$A_{12} = \delta(m_1 + m_2) + 2\left(\sqrt{1 - m_1\delta}\,\sqrt{1 - m_2\delta}\right) - 2, \tag{35}$$

$$A_{i3} = -2a_3 - 4\gamma a_3^3 + \delta a_3 m_i + \delta m_3 a_3 + 2\left(\sqrt{1 - m_i\delta}\,\sqrt{a_3^2(\gamma a_3^2 - \delta m_3 + 1)}\right), (i = 1, 2), \quad (36)$$

$$\eta_i = x + m_i\, y - \left(\frac{1}{2} m_i \alpha + \sqrt{1 + \gamma - m_i \delta}\right)\, t,\, i = 1, 2, \quad (37)$$

and

$$\theta_3 = a_3 x + m_3 a_3 y - \left(\frac{1}{2}\alpha m_3 a_3 + \sqrt{\gamma a_3^4 - \delta m_3 a_3^2 + a_3^2}\right) t. \quad (38)$$

Setting the constraint parameters $m_1 = m_2^* = 1 + I$, $m_3 = -0.5$, and $a_3 = 0.5$ to Eqs. (34)-(38), one can see the elastic interaction between one lump soliton and one stripe soliton in **Fig. 8**. **Figs. 8(a$_1$)-8(a$_5$)** illustrate the 3D plots in the (x, y)-plane at $t = -20$, $t = -10$, $t = 0$, $t = 10$, $t = 20$, respectively, whereas **Figs. 8(b$_1$)-8(b$_5$)** demonstrate the density views of **Figs. 8(a$_1$)-8(a$_5$)**, respectively. At $t = -20$, lump soliton appears in the negative side of the x-axis and is separated from the line soliton (see **Fig. 8(a$_1$)**). It can be also seen from **Figs. 8(a$_2$)-(a$_3$)** that the lump soliton is gradually integrated with the soliton as time goes on ($t = -10, 0$). Furthermore, as the time increases ($t = 10, 20$), the lump soliton gradually appears on the positive side of the x-axis and is separated from the line soliton, which can clearly be observed from **Figs. 8(a$_4$)-(a$_5$).** During the propagation, the amplitude of the lump soliton is found to be unchanged. The mentioned behaviors can be clarified from the corresponding density views displayed in **Figs. 8(b$_1$)-8(b$_5$)**.

The overview of restrictions of parameters for localized waves and their interaction solutions among three solitons of Eq. (3) are presented in **Table 2**. The first column in **Table 2** shows the order of N-soliton, while the second column shows the types of localized wave solutions. The last column provides the corresponding restrictions of parameters for the interaction of localized wave solutions.

Table 2. The nonlinear localized wave interaction structures of N-soliton solutions

N-soliton	Localized waves and interaction structures	Constraints
$N=3$	Three stripe solitons	$a_i = p_i, b_i = q_i$, $(i = 1,2,3)$, and $\omega_1 = \omega_2 = \omega_3 = 0$. For cross intersection: $\prod_{i\neq j}(p_i q_j - p_j q_i) \neq 0$; For parallel intersection: $\sum_{i\neq j}(p_i q_j - p_j q_i)^2 = 0$; For cross and parallel intersection: $\prod_{i\neq j}(p_i q_j - p_j q_i) = 0$, and $\sum_{i\neq j}(p_i q_j - p_j q_i)^2 \neq 0$.
	One stripe soliton + one x-periodic breather	$a_1 = a_2^* = Im_1,\ b_1 = b_2 = p_1,\ a_3 = m_2, b_3 = p_2$, and $\omega_1 = \omega_2 = \omega_3 = 0$.
	One stripe soliton + one y-periodic breather	$a_1 = a_2 = l_1,\ b_1 = b_2^* = Iq_1,\ a_3 = l_2, b_3 = q_2$, and $\omega_1 = \omega_2 = \omega_3 = 0$.
	One stripe soliton + one (x,y)-periodic breather	$a_1 = a_2 = l_1,\ b_1 = b_2^* = p_1 + Iq_1,\ a_3 = l_2, b_3 = p_2$, and $\omega_1 = \omega_2 = \omega_3 = 0$. For cross intersection: $l_1 p_2 - l_2 p_1 \neq 0$, and For parallel intersection: $l_1 p_2 - l_2 p_1 = 0$.
	One stripe soliton + one lump soliton	$b_1 = m_1 a_1,\ b_2 = m_2 a_2, b_3 = m_3 a_3, a_1 = l_1\varepsilon, a_2 = l_2\varepsilon,\ m_1 = m_2^* = p_1 + Iq_1, \omega_1 = \omega_2^* = I\pi, \omega_3 = 0$, and $\varepsilon \to 0$.

3.3 Interaction solutions among four-stripe solitons

The following subsections discuss the interaction solutions among four-stripe solitons to the BqE by their graphical illustrations. To reach such aims, setting $N = 4$ to Eq. (11), one can attain a function for four-soliton solutions given by

$$f_4 = 1 + e^{\theta_1} + e^{\theta_2} + e^{\theta_3} + e^{\theta_4} + a_{12}e^{\theta_1+\theta_2} + a_{13}e^{\theta_1+\theta_3} + a_{14}e^{\theta_1+\theta_4} + a_{23}e^{\theta_2+\theta_3} +$$
$$+a_{24}e^{\theta_2+\theta_4} + a_{34}e^{\theta_3+\theta_4} + a_{123}e^{\theta_1+\theta_2+\theta_3} + a_{124}e^{\theta_1+\theta_2+\theta_4} + a_{134}e^{\theta_1+\theta_3+\theta_4} +$$
$$a_{234}e^{\theta_2+\theta_3+\theta_4} + a_{1234}e^{\theta_1+\theta_2+\theta_3+\theta_4}, \quad (39)$$

where θ_i and a_{ij} are specified by Eqs. (12) and (13), respectively, and the phase shifts follow $a_{123} = a_{12}a_{23}a_{13}$ and $a_{1234} = a_{12}a_{13}a_{14}a_{23}a_{24}a_{34}$.

Plugging Eq. (39) into Eq. (14), four-stripe solitons of Eq. (3) can be found in the following form:

$$u = \frac{6\gamma}{\beta}(\ln f_4)_{xx}. \quad (40)$$

On restricting certain conditions on the given parameters and a long-wave limit approach, one can achieve several types of localized interaction solutions. The construction procedure of the localized interaction solutions is described as follows:

Case I: Interaction among two-stripe solitons and one periodic breather

For Eq. (40), if we take $a_1 = a_2^* = l_1 + Im_1$, $b_1 = b_2^* = p_1 + Iq_1$, $a_3 = l_2$, $a_4 = l_3$, $b_3 = p_2$, $b_4 = p_3$, and $\omega_1 = \omega_2 = \omega_3 = \omega_4 = 0$, the four-stripe soliton solutions will degenerate into the interaction among two-stripe solitons and one periodic breather wave solutions. For different values of l_1, m_1, p_1, q_1, l_2, l_3, p_2, and p_3, the periodic breather can move along a line parallel to the x or y axes or its cross-sectional direction. More specifically, three assumptions can be made, such as the interaction among (i) two-stripe solitons and one x-periodic breather, (ii) two-stripe solitons and one y-periodic breather, and (iii) two-stripe solitons and one xy-periodic breather. **Figs. 9(a)-(f)** present such types of interaction solutions in the (x, y)-plane.

(i) Setting $a_1 = a_2^* = 0.50I$, $a_3 = 0.50$, $a_4 = 0.75$, $b_1 = b_2 = 0.25$, $b_3 = 0.25$, $b_4 = 0.75$, $\omega_1 = 0$, $\omega_2 = 0$, $\omega_3 = 0$, $\omega_4 = 0$, $\alpha = 1$, $\beta = 1$, $\gamma = 1$, and $\delta = 1$ in the class of solutions given by Eq. (40), one can characterize the interaction solution among two-stripe solitons and one x-periodic breather. Such characteristics are illustrated by their 3D and respective density views displayed in **Figs. 9(a)** and **9(d)**, respectively. It is seen from the imposing constraint values that the breather wave is parallel to the x-axis when a_1 and a_2 are purely imaginary numbers and the others are real numbers.

(ii) Substituting $a_1 = a_2 = 0.25$, $a_3 = 0.25$, $a_4 = 0.50$, $b_1 = b_2^* = 0.45I$, $b_3 = 0.50$, $b_4 = 0.50$, $\omega_1 = 0$, $\omega_2 = 0$, $\omega_3 = 0$, $\omega_4 = 0$, $\alpha = 1$, $\beta = 1$, $\gamma = 1$, and $\delta = 1$ in the class of solutions specified by Eq. (40), one can represent the interaction solutions among two-stripe solitons and one y-periodic breather. These behaviors are exhibited by their 3D and density plots through **Fig. 9(b)** and **Fig. 9(c)**, respectively. When b_1 and b_2 are purely imaginary numbers, and the others are real numbers, the breather wave is periodic only along the y-axis.

(iii) Putting $a_1 = a_2 = \frac{1}{3}$, $a_3 = \frac{1}{3}$, $a_4 = \frac{1}{3}$, $b_1 = b_2^* = -0.3 + I$, $b_3 = 0.8$, $b_4 = 0.25$, $\omega_1 = 0$, $\omega_2 = 0$, $\omega_3 = 0$, $\omega_4 = 0$, $\alpha = 1$, $\beta = 1$, $\gamma = 1$, and $\delta = 1$ in the class of solutions given by Eq. (40), one can expose the interaction solution among two-stripe solitons and one y-periodic breather. These behaviors are exposed by their 3D and density plots through **Figs. 9(c)** and **9(e)**, respectively. In such cases, b_1, b_2 are imaginary numbers and the remaining are real numbers.

Case II: Interaction between two periodic breathers

The class of solutions presented by Eq. (40) expresses the interaction between two parallel x-periodic breathers, when we set the constraint parameters as $a_1 = a_2^* = 0.50I$, $a_3 = a_4^* = 0.50I$, $b_1 = b_2 = 0.3$, $b_3 = b_4 = 0.50$, $\omega_1 = 0$, $\omega_2 = 0$, $\omega_3 = 0$, $\omega_4 = 0$, $\alpha = 1$, $\beta = 1$, $\gamma = 1$, and $\delta = 1$. Two parallel x-periodic breathers are displayed in **Figs. 10(a)** and **10(d)** through the 3D and its density graphs. The interaction between two parallel x-periodic breathers turns into two parallel y-periodic breathers when we set $a_1 = a_2 = 0.25$, $a_3 = a_4 = 0.50$, $b_1 = b_2^* = -0.50I$, $b_3 = b_4^* = 0.50I$, $\omega_1 = 0$, $\omega_2 = 0$, $\omega_3 = 0$, $\omega_4 = 0$, $\alpha = 1$, $\beta = 1$, $\gamma = 1$, $\delta = 1$ in Eq. (40). These behaviors are illustrated in **Figs. 10(b)** and **10(e)**. Now, considering $a_1 = a_2 = 0.35$, $a_3 = a_4 = 0.2$, $b_1 = b_2^* = 0.35 - 0.50I$, $b_3 = b_4^* = -0.25 + 0.75I$, $\omega_1 = 0$, $\omega_2 = 0$, $\omega_3 = 0$, $\omega_4 = 0$, $\alpha = 1$, $\beta = 1$, $\gamma = 1$, $\delta = 1$ in Eq. (40), one can attain the interaction between two cross xy-periodic breathers as shown in **Figs. 10(c)** and **10(f)**. It can be observed from the above figures that two breathers retain their velocities and shapes unchanged during propagation. The propagation behavior is not displayed due to the sake of conciseness. However, it is not so difficult to perceive that their interaction is elastic. That means, two periodic breathers only exchange their positions after this elastic collision procedure.

Case III: Interaction among one lump soliton, one periodic breather, and two solitons

In order to explore the interaction solutions among one lump soliton and one periodic breather, and one lump soliton and two solitons for Eq. (3), the constraint parameters a_i, b_i, and ω_i guarantee to satisfy the following conditions for Eq. (40) along with Eq. (39):

$$b_i = m_i a_i \ (i = 1, 2, 3, 4), a_1 = l_1\varepsilon, a_2 = l_2\varepsilon, \omega_1 = \omega_2^* = I\pi, \text{and } \omega_3 = \omega_4 = 0. \quad (41)$$

Inserting the values provided by Eq. (41) into Eq. (39), one can rewrite the function f_4 as follows:

$$f_4 = (A_{12} + \eta_1\eta_2)\, l_1 l_2 \varepsilon^2 + (\eta_1\eta_2 + A_{23}\eta_1 + A_{13}\eta_2 + A_{12} + A_{13}A_{23})e^{\theta_3}\, l_1 l_2 \varepsilon^2 + (\eta_1\eta_2 + A_{24}\eta_1 + A_{14}\eta_2 + A_{12} + A_{14}A_{24})e^{\theta_4}\, l_1 l_2 \varepsilon^2 + A_{34}[\eta_1\eta_2 + (A_{23}+A_{24})\eta_1 + (A_{13}+A_{14})\eta_2 + A_{12} + (A_{13}+A_{14})(A_{23}+A_{24})] \times e^{(\theta_3+\theta_4)}\, l_1 l_2 \varepsilon^2 + O(\varepsilon^3). \quad (42)$$

Taking the long-wave limit as $\varepsilon \to 0$ in Eq. (42), the class of interaction solutions between one lump and one stripe soliton of Eq. (3) can be obtained from Eq. (40), which is given by

$$u = \frac{6\gamma}{\beta}\Big(ln\Big((A_{12} + \eta_1\eta_2) + (\eta_1\eta_2 + A_{23}\eta_1 + A_{13}\eta_2 + A_{12} + A_{13}A_{23})e^{\theta_3} + (\eta_1\eta_2 + A_{24}\eta_1 + A_{14}\eta_2 + A_{12} + A_{14}A_{24})e^{\theta_4} + A_{34}[\eta_1\eta_2 + (A_{23}+A_{24})\eta_1 + (A_{13}+A_{14})\eta_2 + A_{12} + (A_{13}+A_{14})(A_{23}+A_{24})] \times e^{(\theta_3+\theta_4)}\ \Big)\Big)_{xx}, \quad (43)$$

where

$$\eta_i = x + m_i\, y - \left(\frac{1}{2}m_i\alpha + \sqrt{1 + \gamma - m_i\delta}\right)\, t, \ i = 1, 2, \quad (44)$$

$$A_{12} = \delta(m_1 + m_2) + 2\left(\sqrt{1 - m_1\delta}\,\sqrt{1 - m_2\delta}\right) - 2, \quad (45)$$

$$A_{kr} = -2a_r - 4\gamma a_r^3 + \delta a_r m_k + \delta m_r a_r + 2\left(\sqrt{1 - m_k\delta}\,\sqrt{a_r^2(\gamma a_r^2 - \delta m_r + 1)}\right), (k = 1, 2; r = 3,4), \quad (46)$$

$$A_{34} = \frac{2+4\gamma a_3^2-6\gamma a_3^2 a_4+4\gamma a_4^2+\delta m_4+\delta m_4-2\left(\sqrt{(\gamma a_3^2-\delta m_3+1)}\,\sqrt{(\gamma a_4^2-\delta m_4+1)}\right)}{2+4\gamma a_3^2+6\gamma a_3^2 a_4+4\gamma a_4^2+\delta m_4+\delta m_4-2\left(\sqrt{(\gamma a_3^2-\delta m_3+1)}\,\sqrt{(\gamma a_4^2-\delta m_4+1)}\right)}, \quad (47)$$

and

$$\theta_i = a_i x + m_i a_i y - \left(\frac{1}{2}\alpha m_i a_i + \sqrt{\gamma a_i^4 - \delta m_i a_i^2 + a_i^2}\right)t, \ i = 3, 4. \quad (48)$$

(i) Considering $m_1 = m_2^* = p_1 + Iq_1$, $m_3 = m_4^* = p_2 + Iq_2$, and $a_3 = a_4 = \vartheta_1$ in Eqs. (43)–(48), the class of solutions specified by Eq. (43) expresses the interaction solutions between one lump and one breather wave. In particular, taking $p_1 = 0.5$, $q_1 = 1.5$, $p_2 = 0$, $q_2 = 0.75$, $\vartheta_1 = -0.25$, $\alpha = 1$, $\beta = 1$, $\gamma = 1$, $\delta = 1$, the specific structures of the interaction between one lump and one breather are displayed in **Fig. 11**. **Figs. 11(a1)-(a5)** illustrate the 3D plots of the specific solution obtained from Eq. (43) at $t = -40$, $t = -20$, $t = 0$, $t = 20$, $t = 40$, respectively, whereas **Figs. 11(b1)-(b5)** display the corresponding density views of **Figs. 11(a1)-(a5).** At time $t = -40$, the lump soliton is found on the negative side of the x -axis, while the breather is found on the positive side of the x -axis. With the evolution of time ($t = -20, 0, 20, 40$), both breather and lump soliton propagate and change their positions. Thus, it is clear from the wave propagation behaviors (**Figs. 11(a1)-(a5)** or **Figs. 11(b1)-(b5)**) that the interaction structures among the solitons mentioned above is completely elastic.

(ii) When selecting $m_1 = m_2^* = p_1 + Iq_1$, $m_3 = p_2$, $m_4 = p_3$, and $a_3 = a_4 = \vartheta_1$ to Eqs. (43)-(48), the solution given by Eq. (43) is reduced to the interaction among one lump and two-stripe solitons. Taking the particular values of the constraint parameters as $p_1 = 0.75$, $q_1 = 0.75$, $p_2 = -2$, $p_3 = -1$, $\vartheta_1 = -0.6$, $\alpha = 1$, $\beta = 1$, $\gamma = 1$, $\delta = 1$, the aforesaid interaction soliton solution is displayed in **Fig. 12.** The interaction among the solitons is also elastic. It is remarkable to mention here that if we set $p_1 = 0.75$, $q_1 = 0.75$, $p_2 = -1$, $p_3 = -1$, $\vartheta_1 = -0.6$, $\alpha = 1$, $\beta = 1$, $\gamma = 1$, $\delta = 1$ in the solution prescribed by Eq. (43), it turns into the interaction between one lump and one-stripe solitons.

Case IV: Interaction between two lump solitons

In order to search the interaction solutions between two lump solitons for Eq. (3), the constraint parameters a_i, b_i, and ω_i allow to satisfy the following conditions for Eq. (40) along with Eq. (39):

$$b_i = m_i a_i \ (i = 1, 2, 3, 4),\ a_i = l_i \varepsilon \ (i = 1, 2, 3, 4),\ \omega_1 = \omega_2^* = I\pi, \text{ and } \omega_3 = \omega_4^* = I\pi. \quad (49)$$

Substituting the values provided by Eq. (49) into Eq. (39), the function f_4 can be brought as follows:

$$f_4 = (\eta_1\eta_2\eta_3\eta_4 + A_{34}\eta_1\eta_2 + A_{24}\eta_1\eta_3 + A_{23}\eta_1\eta_4 + A_{14}\eta_2\eta_3 + A_{13}\eta_2\eta_4 + A_{12}\eta_3\eta_4 + A_{12}A_{34} + A_{13}A_{24} + A_{14}A_{23})\, l_1 l_2 l_3 l_4 \varepsilon^4 + O(\varepsilon^5). \quad (50)$$

Taking the long-wave limit as $\varepsilon \to 0$ in Eq. (50), the interaction between one lump and one stripe soliton solutions of Eq. (3) can be obtained from Eq. (40), which leads to

$$u = \frac{6\gamma}{\beta}\left(ln(\eta_1\eta_2\eta_3\eta_4 + A_{34}\eta_1\eta_2 + A_{24}\eta_1\eta_3 + A_{23}\eta_1\eta_4 + A_{14}\eta_2\eta_3 + A_{13}\eta_2\eta_4 + A_{12}\eta_3\eta_4 + A_{12}A_{34} + A_{13}A_{24} + A_{14}A_{23}\ )\right)_{xx}, \quad (51)$$

where

$$\eta_i = x + m_i\, y - \left(\frac{1}{2}m_i\alpha + \sqrt{1+\gamma-m_i\delta}\right)\, t,\ i = 1,2,3,4, \quad (52)$$

$$A_{ij} = \delta\left(m_i + m_j\right) + 2\left(\sqrt{1-m_i\delta}\,\sqrt{1-m_j\delta}\right) - 2,\ (1 \le i \le j \le 4). \quad (53)$$

The class of solutions indicated by Eq. (51) expresses two lump solitons. Considering $m_1 = m_2^* = -1 + I$, $m_3 = m_4^* = -1 + 10I$, $\alpha = 1$, $\beta = 1$, $\gamma = 1$, $\delta = 1$ in Eq. (51), the propagation and time evolution of 3D plots of the elastic interaction between two lump solitons are shown in **Figs. 13(a)-13(f)** for time variation $t = -50$, $t = -25$, $t = 0$, $t = 25$, $t = 50$, respectively**.** At $t = -50$, two lump solitons appear on the negative side of the x-axis with different amplitudes (see **Fig. 13(a)**)**.** With the evolution of time ($t = -25, 0, 25, 50$), two lump solitons propagate from the negative side of the x-axis to its positive side, which is clearly realized from **Figs. 13(b)-(f)**. It can be visualized from **Figs. 13(a)-(f)** that the two lumps propagate with the same velocity along the x-axis. During the propagation, the two lumps get closer, then collide with each other, and finally move apart. It is also perceived from the figures that during the propagation, two lumps preserve their amplitudes, but they altered their positions. The overview of the constraint parameters for the four-soliton solutions of Eq. (3) is presented in **Table 3**. The first column in **Table 3** shows the order of N-soliton, the second column shows the localized wave structures, and the last column provides the corresponding parameters of the localized wave interaction solutions in the second column.

Table 3. The nonlinear localized wave interaction structures of N-soliton solutions

N-soliton	Localized waves and interaction structures	Constraints
$N=4$	Two stripe solitons + one y-periodic breather	$a_1=a_2=l_1, b_1=b_2^*=Iq_1, a_3=l_2, a_4=l_3, b_3=p_2, b_4=p_3$, and $\omega_1=\omega_2=\omega_3=\omega_4=0$.
	Two stripe solitons + one x-periodic breather	$a_1=a_2^*=Im_1, b_1=b_2=p_1, a_3=m_2, a_4=m_3, b_3=p_2, b_4=p_3$, and $\omega_1=\omega_2=\omega_3=\omega_4=0$.
	Two stripe solitons + one (x,y)-periodic breather	$a_1=a_2=l_1, b_1=b_2^*=p_1+Iq_1, a_3=l_2, a_4=l_3, b_3=p_2, b_4=p_3$, and $\omega_1=\omega_2=\omega_3=\omega_4=0$.
	Two parallel y-periodic breathers	$a_1=a_2=l_1, b_1=b_2^*=Iq_1, a_3=a_4=l_2, b_3=b_4^*=Iq_2$, and $\omega_1=\omega_2=\omega_3=\omega_4=0$.
	Two parallel x-periodic breathers	$a_1=a_2^*=Im_1, b_1=b_2=p_1, a_3=a_4^*=Im_2, b_3=b_4=p_2$, and $\omega_1=\omega_2=\omega_3=\omega_4=0$.
	Two cross (x,y)-periodic breathers	$a_1=a_2=l_1, b_1=b_2^*=p_1+Iq_1, a_3=a_4=l_2, b_3=b_4^*=p_2+Iq_2$, and $\omega_1=\omega_2=\omega_3=\omega_4=0$.
	One y-periodic breather + one (x,y)-periodic breather	$a_1=a_2=l_1, b_1=b_2^*=Iq_1, a_3=a_4=l_2, b_3=b_4^*=p_2+Iq_2$, and $\omega_1=\omega_2=\omega_3=\omega_4=0$.
	One x-periodic breather + one (x,y)-periodic breather	$a_1=a_2^*=Im_1, b_1=b_2=p_1, a_3=a_4=m_2, b_3=b_4^*=p_2+Iq_2$, and $\omega_1=\omega_2=\omega_3=\omega_4=0$.
	One x-periodic breather + one y-periodic breather	$a_1=a_2^*=Im_1, b_1=b_2=p_1, a_3=a_4=m_2, b_3=b_4^*=Iq_2$, and $\omega_1=\omega_2=\omega_3=\omega_4=0$.
	Two lump solitons	$b_1=m_1a_1, b_2=m_2a_2, b_3=m_3a_3, b_4=m_4a_4, a_1=l_1\varepsilon_1, a_2=l_2\varepsilon_1, a_3=l_3\varepsilon_2, a_4=l_4\varepsilon_2, \omega_1=\omega_2^*=\omega_3=\omega_4^*=I\pi,\ m_1=m_2^*=p_1+Iq_1, m_3=m_4^*=p_2+Iq_2, \varepsilon_1\to 0$, and $\varepsilon_2\to 0$.
	One lump + one periodic breather	$b_1=m_1a_1, b_2=m_2a_2, a_3=a_4=\alpha_2, b_3=b_4^*=p_2+Iq_2, a_1=l_1\varepsilon, a_2=l_2\varepsilon,\ \omega_1=\omega_2^*=I\pi, \omega_3=\omega_4=0,\ m_1=m_2^*=p_1+Iq_1$, and $\varepsilon\to 0$.

4. Discussion of the results and concluding remarks

It is mentioned earlier in the introduction section that Wazwaz and Kaur [52] examined a family of BqEs with distinct dimensions first time. They reported some real and complex multiple soliton solutions by virtue of the simplified Hirota's method. In addition, they also reported a diverse range of soliton solutions in terms of hyperbolic, trigonometric, and rational functions via the exponential expansion scheme. However, in this article, we have used a dependent variable transformation to a dimensionally reduced (2+1)-dimensional BqE and thereby constructed N-soliton solutions via the HBM. Afterward, via the long-wave limit

approach in coordination with certain conditions on the parameters associated with N-solitons, we attained some nonlinear localized waves (soliton, breather, lump, and rogue), and their variety of interaction solutions. To the best of the authors' knowledge, all the localized waves and their variety of interaction solutions are entirely new and reported for the first time.

In order to illustrate the physical significance of the dimensionally reduced (2+1)-dimensional BqE specified by Eq. (3), we have displayed the 3D plots and their corresponding density views to some of the acquired solutions, which represent the solitons, breathers, lumps, rogue waves, and their interactions. The interactions can occur among one stripe and one breather, one stripe and one lump, two stripes and one breather, one lump and one periodic breather, two stripes and one lump, two breathers, and two lumps. It is mentioned that the 3D plots and their density views are made by Maple software of some of the explored validated solutions with suitable values of the constraint parameters. N-soliton solutions of Eq. (3) given by Eq. (14) are presented in **Fig. 1**. It is apparent from **Fig. 1** that the interactions among N-soliton solutions are completely elastic. For $N = 2$, the cross-stripe, one periodic breather, and one lump soliton are obtained, which are illustrated in **Figs. 2-5**. For $N = 3$, we obtained the interaction solutions among three soliton solutions, viz. two parallel-stripe solitons and one soliton, one stripe and periodic breather, and one stripe and one lump solitons by selecting some special parameters, as shown in **Figs. 6- 8**, respectively. In addition, for $N = 4$, we have also attained the interaction solutions among four soliton solutions, such as two-stripe solitons and one periodic breather, two periodic breathers, one lump and one periodic breather, one lump and two-stripe solitons, and two lump solitons. The mentioned interaction solutions among four solitons are justified through **Figs. 9-13**. It is pinpoint to mention here that the lump solitons and rogue waves are obtained via the long-wave limit approach imposing some constraint parameters (see Ablowitz and Satsuma [58]). For other solitons, the HBM along with certain conditions on some constraint parameters are employed. Some of the interaction

582 solutions of the localized waves are presented and their dynamical features are analyzed
583 through some time evolution plots (see **Figs. 6-7** and **Figs. 11-13**). It is clear clearly from the
584 mentioned time evolution plots that all the wave interactions among solitons are elastic. It is
585 also to be mentioned here that all the reported solutions in this article have diverse structures
586 over the solutions available in the literature, and the choice of the constraint parameters has a
587 great influence on the attained solutions and their propagation behaviors. **Tables 1-3** show
588 some mathematical conditions to secure the localized waves and their interaction solutions
589 from the two-soliton, three-soliton, and four-soliton solutions of Eq. (3) on how to select
590 appropriate constraint parameters. It should be pointed out here that no interaction solutions
591 for $N \geq 5$ are explained due to the limitations of our computational scope. However, our future
592 study will concentrate on constructing interaction solutions for the higher values of N, and will
593 present how to select some more appropriate constraint parameters for their interaction
594 solutions. The exhibited results reveal that the acquired solitons might be helpful for explaining
595 the wave propagation behavior in shallow water surfaces. The executed approach can be used
596 to determine localized waves and their interaction solutions to any other NLEEs arising in
597 shallow water.
598

Compliance with ethical standards

This article does not contain any studies with human or animal subjects.

Conflict of interests.

The authors declare that they have no known competing financial interests or personal relationships that could have appeared to influence the work reported in this paper.

CRediT authorship contribution statement

Dipankar Kumar: Conceptualization, Formal analysis, Data curation, Resources, Software, Supervision, Validation, Writing - review editing. **Md. Nuruzzaman**: Methodology, Formal analysis, Software, Writing - original draft. **Gour Chandra Paul** (Corresponding author): Data curation, Methodology, Formal analysis, Resources, Supervision, Validation, Writing - review editing. **Ashabul Hoque**: Formal analysis, Supervision, Validation, Writing - review editing. Finally, all authors have approved this manuscript and take responsibility for the accuracy of its contents.

Data availability statement

Data sharing not applicable to this article as no datasets were generated or analysed during the current study.

Acknowledgments

The work is partially supported by a grant from the University Grants Commission, Bangladesh under grant no. 3632104 through the Bangabandhu Sheikh Mujibur Rahman Science and Technology University, Gopalganj, and the first author acknowledges this support. The research is also supported by the National Science and Technology (NST), Government of Bangladesh by providing NST fellowship under grant Number No. 39.00.0000.012.002.04.19-06 to the second author and the author acknowledges this support.

References

1. Huang, L., Yue, Y., Chen, Y.: Localized waves and interaction solutions to a (3+1)-dimensional generalized KP equation. Comput. Math. Appl.**76**(4). 831–844 (2018)

2. Li, B. X., Borshch, V., Xiao, R. L., Paladugu, S., Turiv, T., Shiyanovskii, S. V., Lavrentovich, O. D.: Electrically driven three-dimensional solitary waves as director bullets in nematic liquid crystals. Nat. Commun. **9**, 2912 (2018)

3. Hirota R. The direct method in soliton theory. 2004, Cambridge University Press, Cambridge. https://doi.org/10.1017/CBO9780511543043

4. Orapine, H. O., Ayankop-Andi, E., Ibeh, G. J.: Analytical and numerical computations of multi-solitons in the Korteweg-de Vries (KdV) equation. Appl. Math. **11**(07), 511 (2020)

5. Zabusky, N. J., Kruskal, M. D.: Interaction of solitons in a collisionless plasma and recurrence of initial states. Phys. Rev. Lett. **15**, 240–243 (1965)

6. Aya, S., Araoka. F.: Kinetics of motile solitons in nematic liquid crystals. Nat. Commun. **11**, 3248 (2020). https://doi.org/10.1038/s41467-020-16864-8

7. Liu, W., Liu, Y., Zhang, Y., Shi, D.: Riemann–Hilbert approach for multi-soliton solutions of a fourth-order nonlinear Schrödinger equation. Mod. Phys. Letts. B. **33**(33), 1950416 (2019)

8. Chabchoub, A., Hoffmann, N.P., Akhmediev, N.: Rogue wave observation in a water wave tank. Phys. Rev. Lett. **106**(20), 204502 (2011)

9. Paul, G. C., Eti, F. Z., Kumar, D.: Dynamical analysis of lump, lump-triangular periodic, predictable rogue and breather wave solutions to the (3+1)-dimensional gKP–Boussinesq equation. Results in Physics. **19**, 103525 (2020)

10. Wu, J., Liu, Y., Piao, L., Zhuang, J., Wang, D. S.: Nonlinear localized waves resonance and interaction solutions of the (3+1)-dimensional Boiti–Leon–Manna–Pempinelli equation. Nonlinear Dyn. **100**, 1527–1541 (2020)

11. Dudley, J.M., Genty, G., Mussot, A., Chabchoub, A., Dias, F.: Rogue waves and analogies in optics and oceanography. Nat. Rev. Phys. **1**(11), 675–689 (2019)

12. Yu, W., Zhang, H., Zhou, Q., Biswas, A., Alzahrani, A. K., Liu, W.: The mixed interaction of localized, breather, exploding and solitary wave for the (3+1)-dimensional Kadomtsev–Petviashvili equation in fluid dynamics. Nonlinear Dyn. **100**(2), 1611–1619 (2020)

13. Nestor, S., Abbagari, S., Houwe, A., Betchewe, G., Doka, S. Y.: Diverse chirped optical solitons and new complex traveling waves in nonlinear optical fibers. Commun. Theor. Phys. **72**(6), 065501 (2020)

14. Xu, T., Chen, Y., Lin, J.: Localized waves of the coupled cubic–quintic nonlinear Schrödinger equations in nonlinear optics. Chin. Phys. B. **26**(12), 120201 (2017)

15. Liu, Y., Wen, X. Y., Wang, D. S.: Novel interaction phenomena of localized waves in the generalized (3+1)-dimensional KP equation. Comput. Math. Appl. **78**(1), 1–9 (2019)

16. Li, Z. Q., Tian, S. F., Peng, W. Q., Yang, J. J.: Inverse Scattering Transform and Soliton Classification of Higher-Order Nonlinear Schrödinger-Maxwell-Bloch Equations. Theor. Math. Phys. **203**(3), 709–725 (2020)

17. Lü, X., Hua, Y. F., Chen, S. J., Tang, X. F.: Integrability characteristics of a novel (2+1)-dimensional nonlinear model: Painlevé analysis, soliton solutions, Bäcklund transformation, Lax pair and infinitely many conservation laws. Commun. Nonlinear Sci. Numer. Simul. **95**, 105612 (2021)

18. Yang, Y., Suzuki, T., Cheng, X.: Darboux transformations and exact solutions for the integrable nonlocal Lakshmanan−Porsezian−Daniel equation. Appl. Math. Letts. **99**, 105998 (2020)

19. Ryabov, P. N., Sinelshchikov, D. I., Kochanov, M. B.: Application of the Kudryashov method for finding exact solutions of the high order nonlinear evolution equations. Appl. Math. Comput. **218**(7), 39653972 (2011)

20. Kumar, D., Seadawy, A. R., Joardar, A. K.: Modified Kudryashov method via new exact solutions for some conformable fractional differential equations arising in mathematical biology. Chin. J. Phys. **56**(1), 75–85 (2018)

21. Kumar, D., Kaplan, M.: Application of the modified Kudryashov method to the generalized Schrödinger–Boussinesq equations. Opt. Quant. Electron. **50**(9), 1–14 (2018)

22. Kumar, D., Paul, G. C., Biswas, T., Seadawy, A. R., Baowali, R., Kamal, M., Rezazadeh, H.: Optical solutions to the Kundu-Mukherjee-Naskar equation: mathematical and graphical analysis with oblique wave propagation. Phys. Scr. **96**(2), 025218 (2020)

23. Ahmed, H. M., Rabie, W. B., Ragusa, M. A.: Optical solitons and other solutions to Kaup–Newell equation with Jacobi elliptic function expansion method. Anal. Math. Phys. **11**(1), 1–6 (2021)

24. Kumar, D., Hosseini, K., Samadani, F.: The sine-Gordon expansion method to look for the traveling wave solutions of the Tzitzéica type equations in nonlinear optics. Optik. **149**, 439–446 (2017)

25. Kumar, D., Manafian, J., Hawlader, F., Ranjbaran, A.: New closed form soliton and other solutions of the Kundu–Eckhaus equation via the extended sinh-Gordon equation expansion method. Optik. **160**, 159–167 (2018)

26. Seadawy, A. R., Kumar, D., Chakrabarty, A. K.: Dispersive optical soliton solutions for the hyperbolic and cubic-quintic nonlinear Schrödinger equations via the extended sinh-Gordon equation expansion method. Eur. Phys. J. Plus. **133**(5), 182 (2018)

27. Kumar, D., Joardar, A. K., Hoque, A., Paul, G. C.: Investigation of dynamics of nematicons in liquid crystals by extended sinh-Gordon equation expansion method. Opt. Quant. Electron. **51**(7), 1–36 (2019)

28. Kumar, D., Paul, G. C.: Solitary and periodic wave solutions to the family of nonlinear conformable fractional Boussinesq-like equations. Math. Meth. Appl Sci. **44**(4), 3138–3158 (2021)

29. Kumar, D., Paul, G. C., Mondal, J., Islam, A. S.: On the propagation of alphabetic-shaped solitons to the (2+1)-dimensional fractional electrical transmission line model with wave obliqueness. Res. Phys. **19**, 103641 (2020)

30. Kumar, D., Park, C., Tamanna, N., Paul, G. C., Osman, M. S.: Dynamics of two-mode Sawada-Kotera equation: Mathematical and graphical analysis of its dual-wave solutions. Res. Phys. **19**, 103581 (2020)

31. Cui, C.J., Tang, X.Y., Cui, Y.J.: New variable separation solutions and wave interactions for the (3+1)-dimensional Boiti–Leon–Manna–Pempinelli equation. Appl. Math. Letts. **102**, 106109 (2020)

32. Wang, D. S., Guo, B., Wang, X.: Long-time asymptotics of the focusing Kundu–Eckhaus equation with nonzero boundary conditions. J. Differ. Equ. **266**(9), 5209–5253 (2019)

33. Kaur, L., Wazwaz, A.M.: Painlevé analysis and invariant solutions of generalized fifth-order nonlinear integrable equation. Nonlinear Dyn. **94**(4), 2469–2477 (2018)

34. Ren, B., Lin, J., Lou, Z. M.: Consistent Riccati expansion and rational solutions of the Drinfel'd–Sokolov–Wilson equation. Appl. Math. Letts. **105**, 106326 (2020)

35. Dong, M.J., Tian, S.F., Yan, X.W., Zou, L.: Solitary waves, homoclinic breather waves and rogue waves of the (3+1)-dimensional Hirota bilinear equation. Comput. Math. Appl. **75**(3), 957–964 (2018)

36. Hua, Y. F., Guo, B. L., Ma, W. X., Lü, X.: Interaction behavior associated with a generalized (2+1)-dimensional Hirota bilinear equation for nonlinear waves. Appl. Math. Modell. **74**, 184–198 (2019)

37. He, B., Meng, Q.: Lump and interaction solutions for a generalized (3+1)-dimensional propagation model of nonlinear waves in fluid dynamics. Int. J. Comput. Math. **98**(3), 592–607 (2021)

38. Kumar, D., Kuo, C. K., Paul, G. C., Saha, J., Jahan, I.: Wave propagation of resonance multi-stripes, complexitons, and lump and its variety interaction solutions to the (2+1)-dimensional pKP equation. Commun. Nonlinear Sci. Numer. Simul. **100**, 105853 (2021)

39. Yue, Y., Huang, L., Chen, Y.: Localized waves and interaction solutions to an extended (3+1)-dimensional Jimbo–Miwa equation. Appl. Math. Letts. **89**, 70–77 (2019)

40. Rao, J., He, J., Mihalache, D., Cheng, Y.: Dynamics and interaction scenarios of localized wave structures in the Kadomtsev–Petviashvili-based system. Appl. Math. Letts. **94**, 166–173 (2019)

41. Liu, Y., Wen, X. Y., Wang, D. S.: The N-soliton solution and localized wave interaction solutions of the (2+1)-dimensional generalized Hirota-Satsuma-Ito equation. Comput. Math. Appl. **77**(4), 947–966 (2019)

42. Zhang, W. J, Xia, T. C.: Solitary wave, M-lump and localized interaction solutions to the (4+1)-dimensional Fokas equation. Phys. Scr. **95**(4), 045217 (2020).

43. Sun, L., Qi, J., An, H.: Novel localized wave solutions of the (2+1)-dimensional Boiti–Leon–Manna–Pempinelli equation. Commun. Theor. Phys. **72**(12), 125009 (2020)

44. Song, N., Xue, H., Xue, Y. K.: Dynamics of higher-order localized waves for a coupled nonlinear Schrödinger equation. Commun. Nonlinear Sci. Numer. Simul. **82**, 105046 (2020)

45. Ma, Y. L.: N-solitons, breathers and rogue waves for a generalized Boussinesq equation. Int. J. Comp. Math. **97**(8), 1648–1661 (2020)

46. Vinodh, D., Asokan, R.: Multi-soliton, rogue wave and periodic wave solutions of generalized (2+1)- dimensional Boussinesq equation. Int. J. Appl. Comput. Math. **6**(1), 1–6 (2020)

47. Liu, W., Zhang, Y.: Dynamics of localized waves and interaction solutions for the (3+1)-dimensional B-type Kadomtsev–Petviashvili–Boussinesq equation. Adv. Differ. Equ. **2020**(1), 1–12 (2020)

48. Yue, Y., Chen, Y.: Dynamics of localized waves in a (3+1)-dimensional nonlinear evolution equation. Mod. Phys. Letts. B. **33**(09), 1950101 (2019)

49. Wazwaz, A. M.: New travelling wave solutions to the Boussinesq and the Klein–Gordon equations. Commun. Nonlinear Sci. Numer. Simul. **13**(5), 889–901 (2008)

50. Jawad, A.M., Petković, M.D., Laketa, P., Biswas, A.: Dynamics of shallow water waves with Boussinesq equation. Scientia Iranica. **20**(1), 179–184 (2013)

51. Lin, Q., Wu, Y. H., Loxton, R., Lai, S.: Linear B-spline finite element method for the improved Boussinesq equation. J. Comput. Appl. Math. **224**(2), 658–667 (2019)

52. Wazwaz, A. M., Kaur, L.: New integrable Boussinesq equations of distinct dimensions with diverse variety of soliton solutions. Nonlinear Dyn. **97**(1), 83–94 (2019)

53. Zou, H., Li, H., Liu, X., Liu, A.: The application of a numerical model to coastal surface water waves. J Ocean Univ. China. **4**(2), 177–184 (2005)

54. Droenen, N., Deigaard, R.: Adaptation of a Boussinesq wave model for dune erosion modeling. Coastal Eng. Proceedings. **33**, 31-31 (2012)

55. Kirby, J, T.: Boussinesq models and their application to coastal processes across a wide range of scales. J. Waterw. Port Coast. Ocean Engrg. **142**(6), (2016)

56. Lynett, P. J., Melby, J. A., Kim, D. H.: An application of Boussinesq modeling to hurricane wave overtopping and inundation. Ocean Eng. **37**(1), 135-153 (2010)

57. Roeber, V., Cheung, K. F., Kobayashi, M. H.: Shock-capturing Boussinesq-type model for nearshore wave processes. Coastal Eng. **57**(4), 407–423 (2010)

58. Ablowitz, M.J., Satsuma, J.: Solitons and rational solutions of nonlinear evolution equations. J. Math. Phys. **19**(10), 2180–2186 (1978)

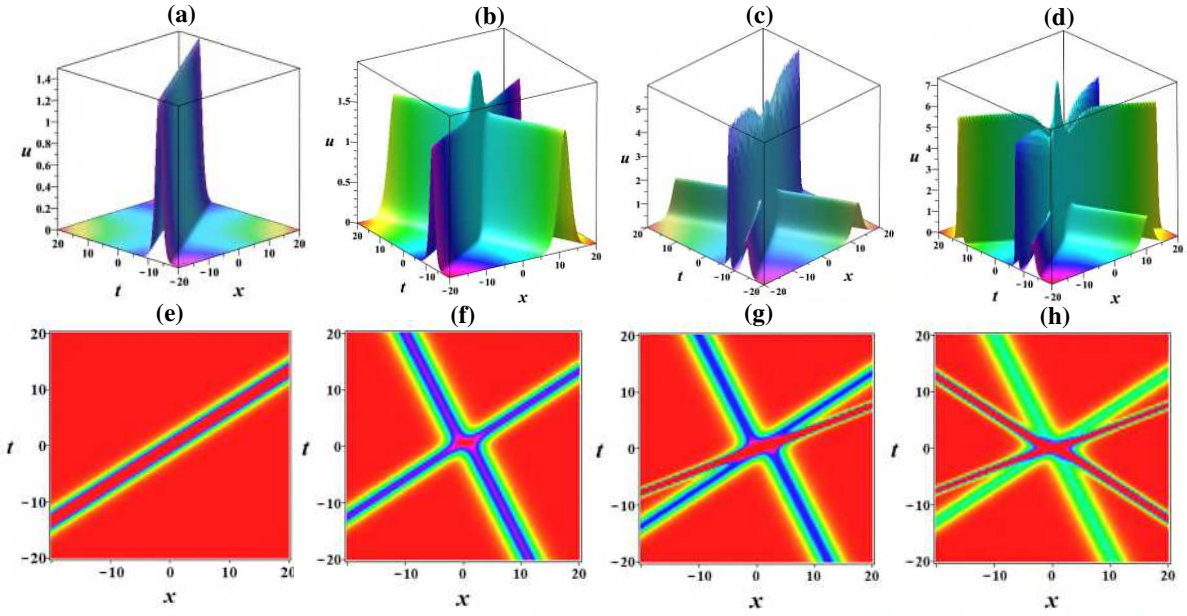

Figure 1. Graphical illustration of N-soliton solutions given by Eq. (14) of Eq. (3) with $a_1 = 1$, $a_2 = -1$, $a_3 = 2$, $a_4 = -2$, $b_1 = 1$, $b_2 = -1$, $b_3 = 2$, $b_4 = -2$, $\omega_1 = 0$, $\omega_2 = 0$, $\omega_3 = 0$, $\omega_4 = 0$, $\alpha = 1$, $\beta = 1$, $\gamma = 1$, $\delta = 1$, and $y = 0$. The 3D plots for (a) $N = 1$, (b) $N = 2$, (c) $N = 3$, and (d) $N = 4$. (e)-(h) The density views of (a)-(d), respectively.

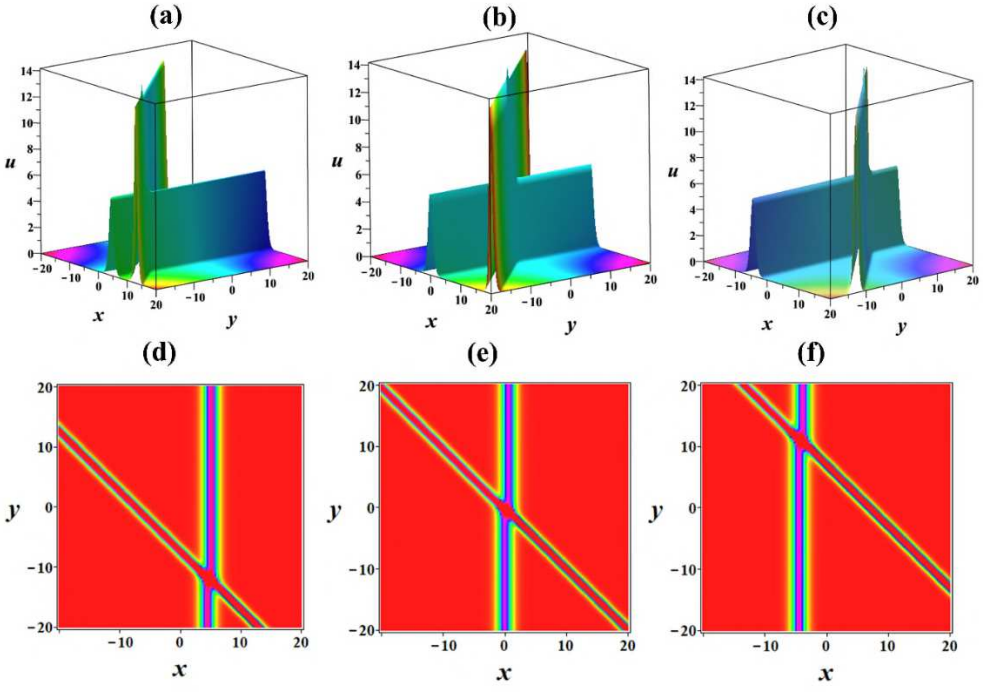

Figure 2. Time evolution 3D plots of two cross-stripe soliton solutions given by Eq. (18) at (a) $t = -5$, (b) $t = 0$, and (c) $t = 5$ with $p_1 = 3$, $p_2 = -2$, $q_1 = 3$, $q_2 = 0$, $\omega_1 = 0$, $\omega_2 = 0$, $\alpha = 1$, $\beta = 1$, $\gamma = 1$, $\delta = 1$. (d)-(f) The density views of (a)-(c), respectively.

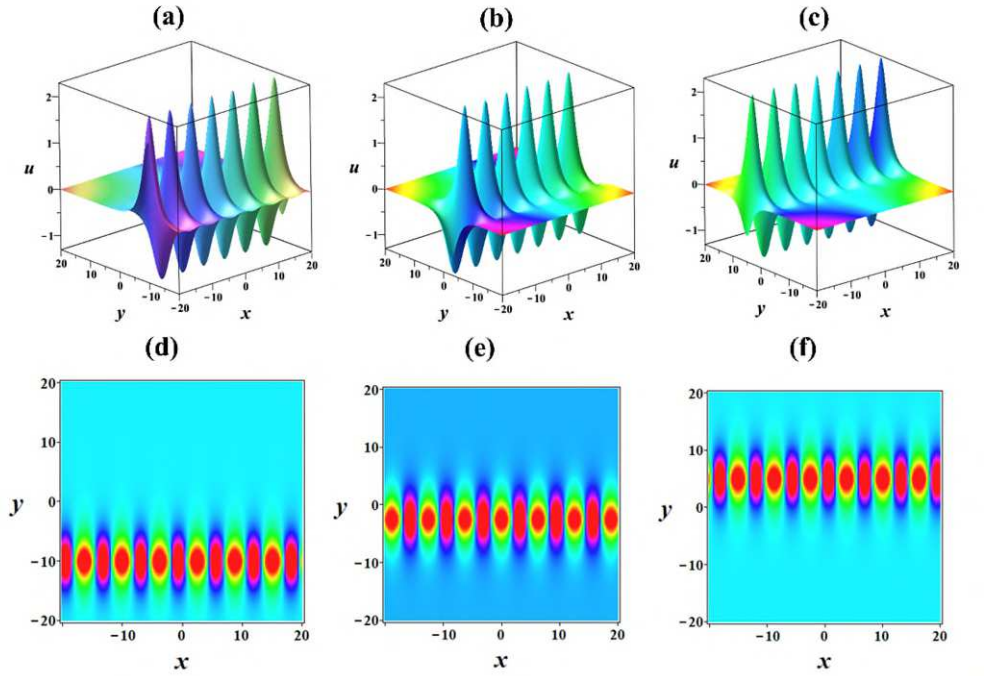

Figure 3. Time evolution 3D plots of one x-periodic breather wave solutions given by Eq. (21) at (a) $t = -5$, (b) $t = 0$, and (c) $t = 5$ with $a_1 = a_2^* = I$, $b_1 = 0.5$, $b_2 = 0.5$, $\omega_1 = 0$, $\omega_2 = 0$, $\alpha = 1$, $\beta = 1$, $\gamma = 1$, $\delta = 1$. (d)-(f) The density views of (a)-(c), respectively.

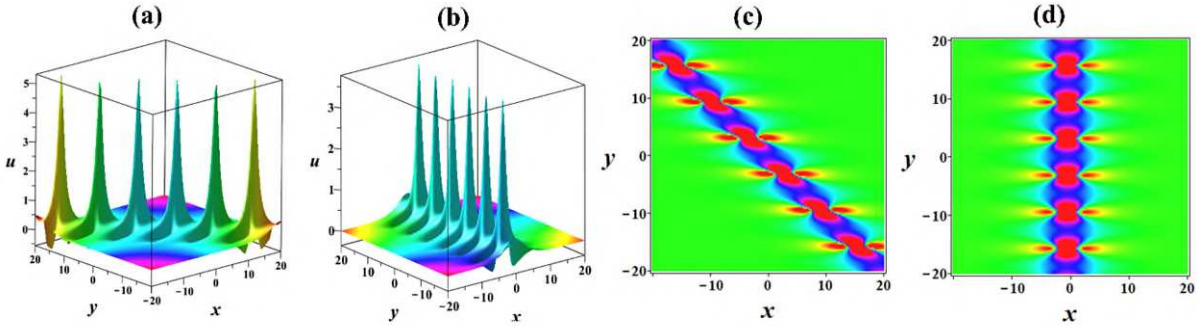

Figure 4. Periodic breather solutions given by Eq. (23) at $t = 0$. The 3D plots of (a) one xy-periodic breather with $a_1 = a_2 = \frac{1}{3}$, $b_1 = b_2^* = \frac{1}{3} + I$, $\omega_1 = \omega_2 = 0$, $\alpha = 1$, $\beta = 1$, $\gamma = 1$, $\delta = 1$, and (b) one y-periodic breather with $a_1 = a_2 = \frac{1}{3}$, $b_1 = b_2^* = I$, $\omega_1 = \omega_2 = 0$, $\alpha = 1$, $\beta = 1$, $\gamma = 1$, $\delta = 1$. (c)-(d) The density views of (a)-(b), respectively.

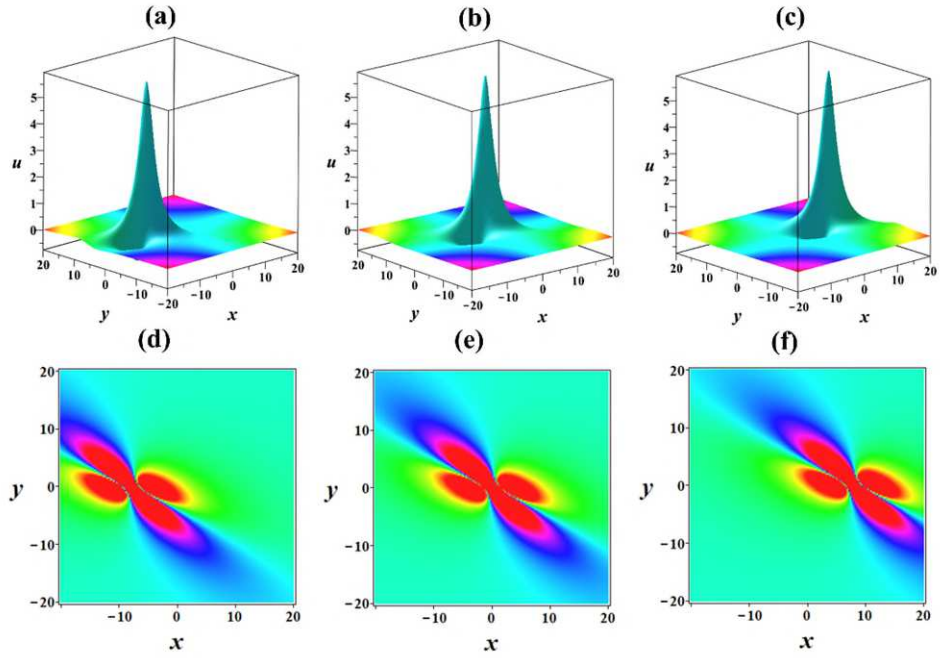

Figure 5. Time evolution 3D plots of lump soliton solutions given by Eq. (25) at (a) $t = -5$, (b) $t = 0$, and (c) $t = 5$ under the specified conditions $m_1 = m_2^* = 1 + I$, $\alpha = 1$, $\beta = 1$, $\gamma = 1$, $\delta = 1$. (d)-(f) The density views of (a)-(c), respectively.

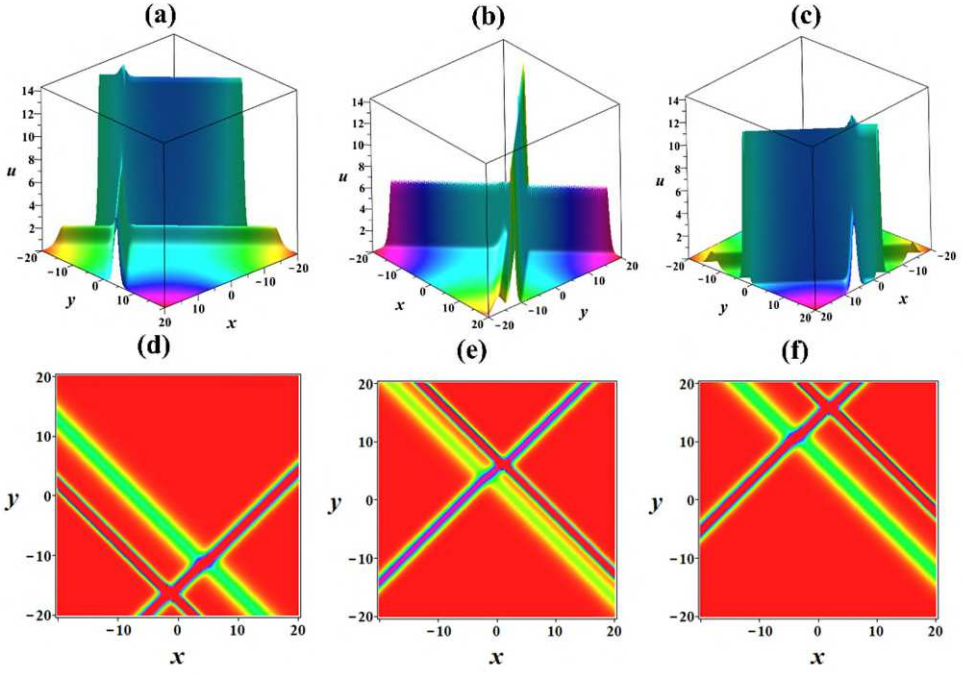

Figure 6. Time evolution 3D plots of the interaction of two parallel-stripe solitons with another soliton given by Eq. (29) at (a) $t = -5$, (b) $t = 2$, and (c) $t = 5$ under suitable selection of constraint parameters as $p_1 = 3$, $p_2 = -2$, $p_3 = 1$, $q_1 = 3$, $q_2 = 2$, $q_3 = 1$, $\omega_1 = 0$, $\omega_2 = 0$, $\omega_3 = 0$, $\alpha = 1$, $\beta = 1$, $\gamma = 1$, $\delta = 1$. (d)-(f) The density views of (a)-(c), respectively.

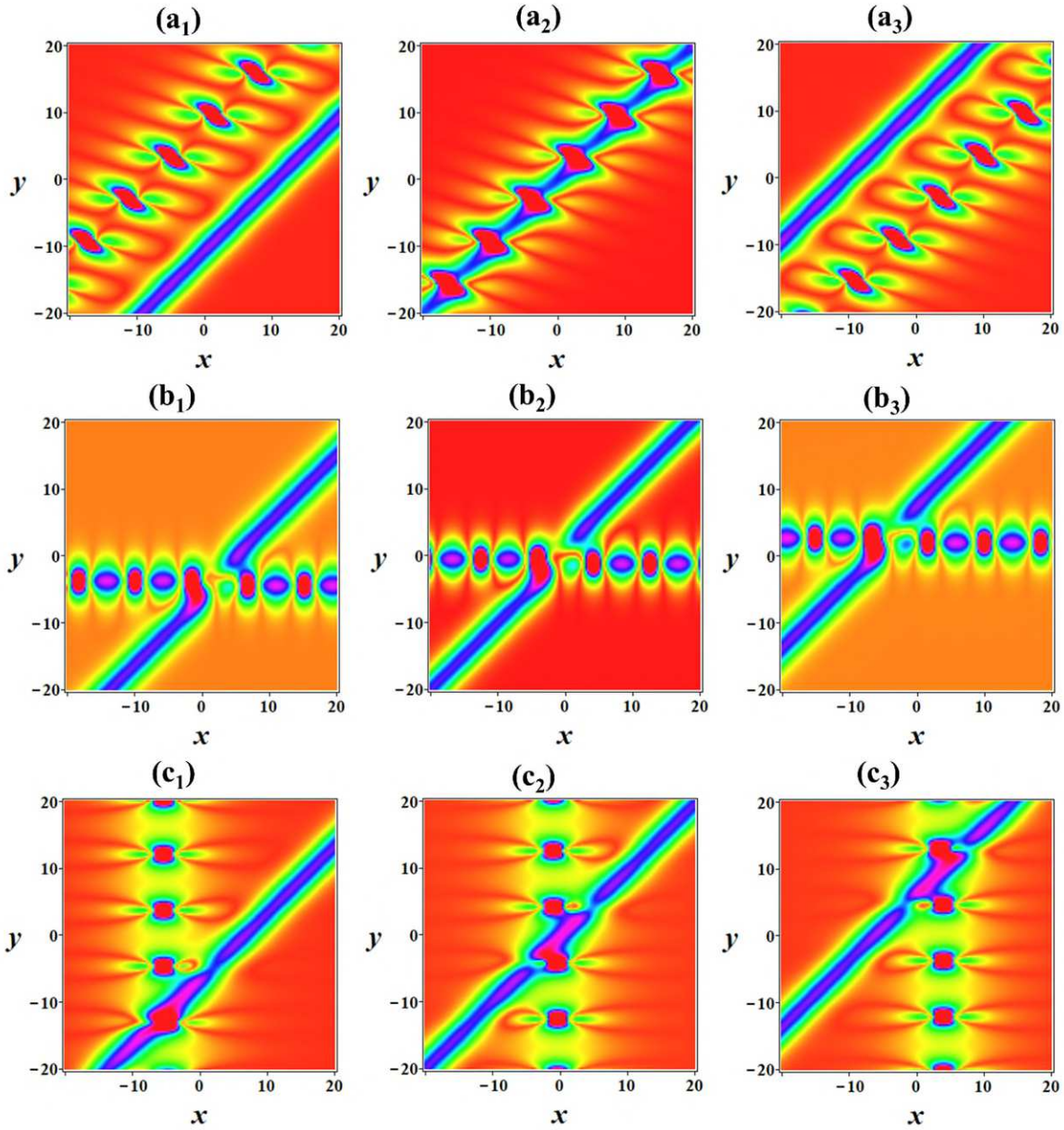

Figure 7. Time evolution density plots of the interaction solutions between one-stripe soliton and one periodic breather given by Eq. (29) at (a1)-(c1) $t = -5$, (a2)-(c2) $t = 0$, and (a3)-(c3) $t = 5$. (a1)-(a3) One stripe soliton and one xy-periodic breather with $a_1 = a_2 = 0.25$, $a_3 = -0.75$, $b_1 = b_2^* = -0.25 + 0.75I$, $b_3 = 0.75$, $\omega_1 = 0$, $\omega_2 = 0$, $\omega_3 = 0$, $\alpha = 1$, $\beta = 1$, $\gamma = 1$, $\delta = 1$, (b1)-(b3) One stripe soliton and one x-periodic breather with $a_1 = a_2^* = 0.25I$, $a_3 = -0.75$, $b_1 = b_2 = -0.25$, $b_3 = 0.75$, $\omega_1 = 0$, $\omega_2 = 0$, $\omega_3 = 0$, $\alpha = 1$, $\beta = 1$, $\gamma = 1$, $\delta = 1$, and (c1)-(c3) One stripe soliton and one y-periodic breather with $a_1 = a_2 = 0.25$, $a_3 = -0.75$, $b_1 = b_2^* = 0.75I$, $b_3 = 0.75$, $\omega_1 = 0$, $\omega_2 = 0$, $\omega_3 = 0$, $\alpha = 1$, $\beta = 1$, $\gamma = 1$, $\delta = 1$.

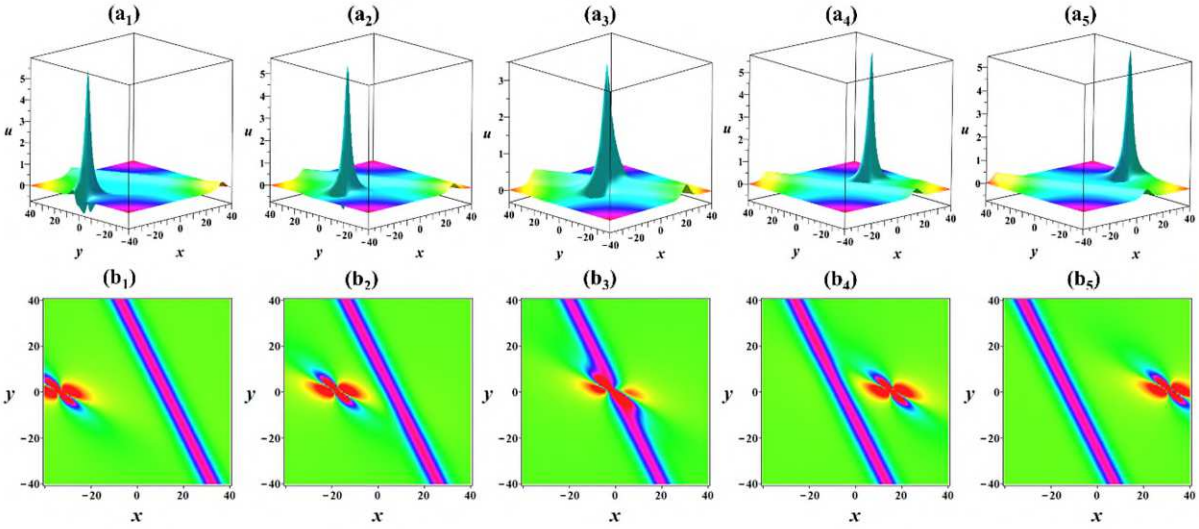

Figure 8. Time evolution 3D plots of lump-stripe solitons given by Eq. (34) at (a$_1$) $t = -20$, (a$_2$) $t = -10$, (a$_3$) $t = 0$, (a$_4$) $t = 10$, and (a$_5$) $t = 20$ with $m_1 = (1 + I)$, $m_2 = (1 - I)$, $m_3 = 0.5$, $a_3 = -0.5$, $\alpha = 1$, $\beta = 1$, $\gamma = 1$, $\delta = 1$. (b$_1$)-(b$_5$) The density views of (a$_1$)-(a$_5$), respectively.

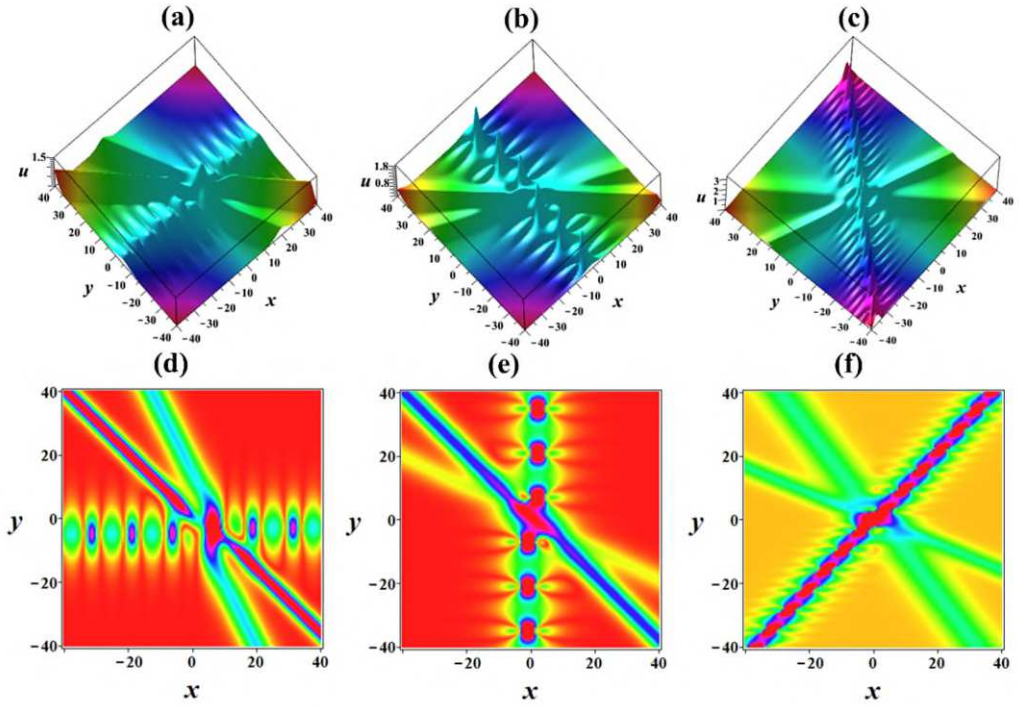

Figure 9. Interaction solutions among two-stripe solitons and one periodic breather given by Eq. (40) at $t = 0$. The 3D plots of (a) two-stripe solitons and one x-periodic breather with $a_1 = a_2^* = 0.50I$, $a_3 = 0.50$, $a_4 = 0.75$, $b_1 = b_2 = 0.25$, $b_3 = 0.25$, $b_4 = 0.75$, $\omega_1 = 0$, $\omega_2 = 0$, $\omega_3 = 0$, $\omega_4 = 0$, $\alpha = 1$, $\beta = 1$, $\gamma = 1$, $\delta = 1$, (b) two-stripe solitons and one y-periodic breather with $a_1 = a_2 = 0.25$, $a_3 = 0.25$, $a_4 = 0.50$, $b_1 = b_2^* = 0.45I$, $b_3 = 0.50$, $b_4 = 0.50$, $\omega_1 = 0$, $\omega_2 = 0$, $\omega_3 = 0$, $\omega_4 = 0$, $\alpha = 1$, $\beta = 1$, $\gamma = 1$, $\delta = 1$, and (c) two-stripe solitons and one xy-periodic breather with $a_1 = a_2 = \frac{1}{3}$, $a_3 = \frac{1}{3}$, $a_4 = \frac{1}{3}$, $b_1 = b_2^* = -0.3 + I$, $b_3 = 0.8$, $b_4 = 0.25$, $\omega_1 = 0$, $\omega_2 = 0$, $\omega_3 = 0$, $\omega_4 = 0$, $\alpha = 1$, $\beta = 1$, $\gamma = 1$, $\delta = 1$. (d)-(f) The density views of (a)-(c), respectively.

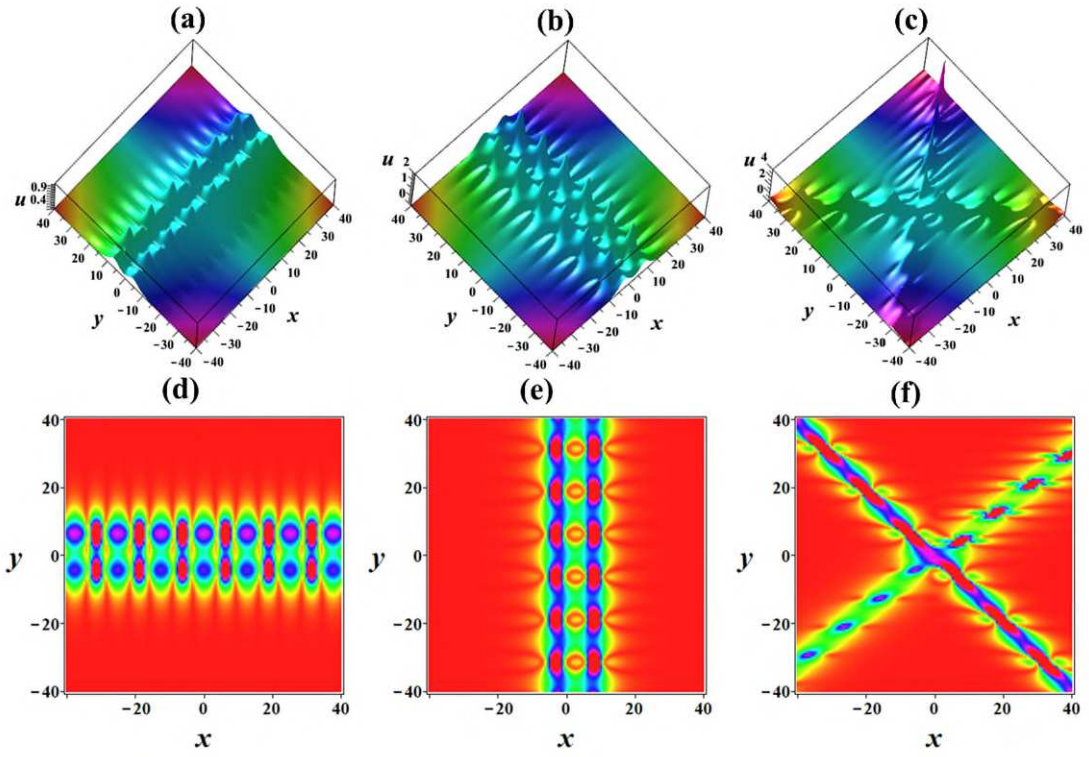

Figure 10. Interaction solutions between two periodic breathers given by Eq. (40) at $t = 0$. The 3D plots of (a) two parallel x-periodic breathers with $a_1 = a_2^* = 0.50I$, $a_3 = a_4^* = 0.50I$, $b_1 = b_2 = 0.3$, $b_3 = b_4 = 0.50$, $\omega_1 = 0$, $\omega_2 = 0$, $\omega_3 = 0$, $\omega_4 = 0$, $\alpha = 1$, $\beta = 1$, $\gamma = 1$, $\delta = 1$, (b) two parallel y-periodic breathers with $a_1 = a_2 = 0.25$, $a_3 = a_4 = 0.50$, $b_1 = b_2^* = -0.50I$, $b_3 = b_4^* = 0.50I$, $\omega_1 = 0$, $\omega_2 = 0$, $\omega_3 = 0$, $\omega_4 = 0$, $\alpha = 1$, $\beta = 1$, $\gamma = 1$, $\delta = 1$, and (c) two cross xy-periodic breathers with $a_1 = a_2 = 0.35$, $a_3 = a_4 = 0.2$, $b_1 = b_2^* = 0.35 - 0.50I$, $b_3 = b_4^* = -0.25 + 0.75I$, $\omega_1 = 0$, $\omega_2 = 0$, $\omega_3 = 0$, $\omega_4 = 0$, $\alpha = 1$, $\beta = 1$, $\gamma = 1$, $\delta = 1$. (d)-(f) The density views of (a)-(c), respectively.

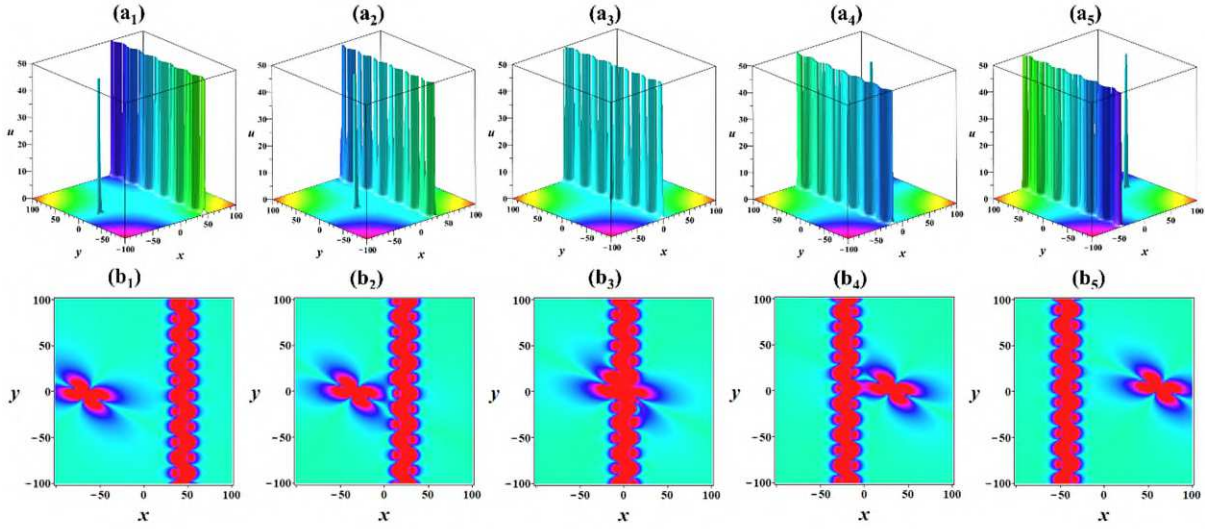

Figure 11. Time evolution 3D plots of the interaction solutions between one lump and one periodic breather given by Eq. (43) at (a_1) $t = -40$, (a_2) $t = -20$, (a_3) $t = 0$, (a_4) $t = 20$, and (a_5) $t = 40$ under constraint parameters as $m_1 = m_2^* = (0.5 + 1.5I)$, $m_3 = m_4^* = 0.75I$, $a_3 = -0.25$, $a_4 = -0.25$, $\alpha = 1$, $\beta = 1$, $\gamma = 1$, $\delta = 1$. (b_1)-(b_5) The density views of (a_1)-(a_5), respectively.

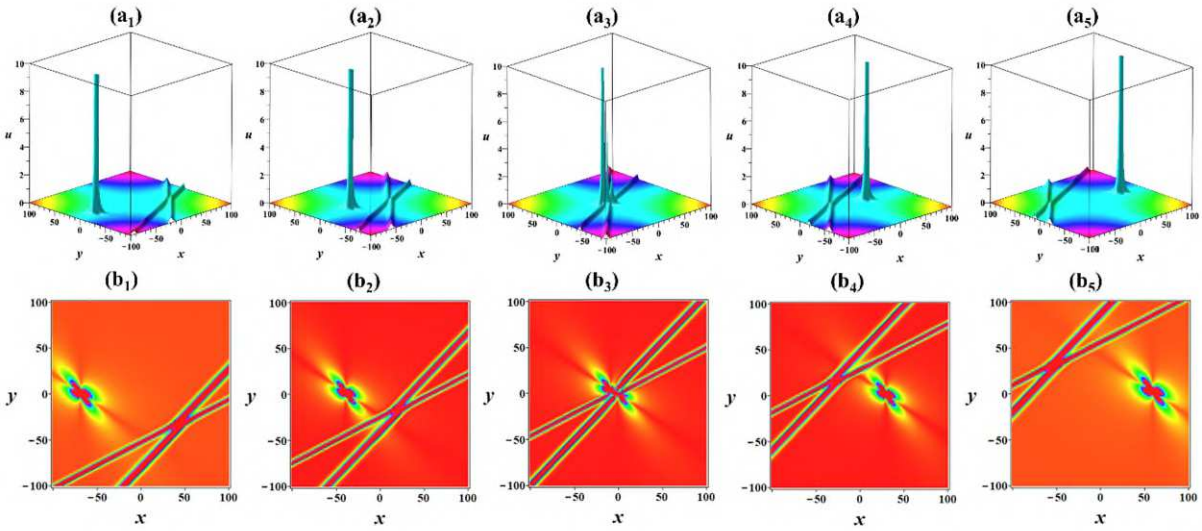

Figure 12. Time evolution 3D plots of the interaction solutions between one lump and two-stripe solitons given by Eq. (43) at (a_1) $t = -40$, (a_2) $t = -20$, (a_3) $t = 0$, (a_4) $t = 20$, and (a_5) $t = 40$ with $m_1 = m_2^* = (0.75 + 0.75I)$, $m_3 = -2$, $m_4 = -1$, $a_3 = -0.6$, $a_4 = -0.6$, $\alpha = 1$, $\beta = 1$, $\gamma = 1$, $\delta = 1$. (b_1)-(b_5) The density views of (a_1)-(a_5), respectively.

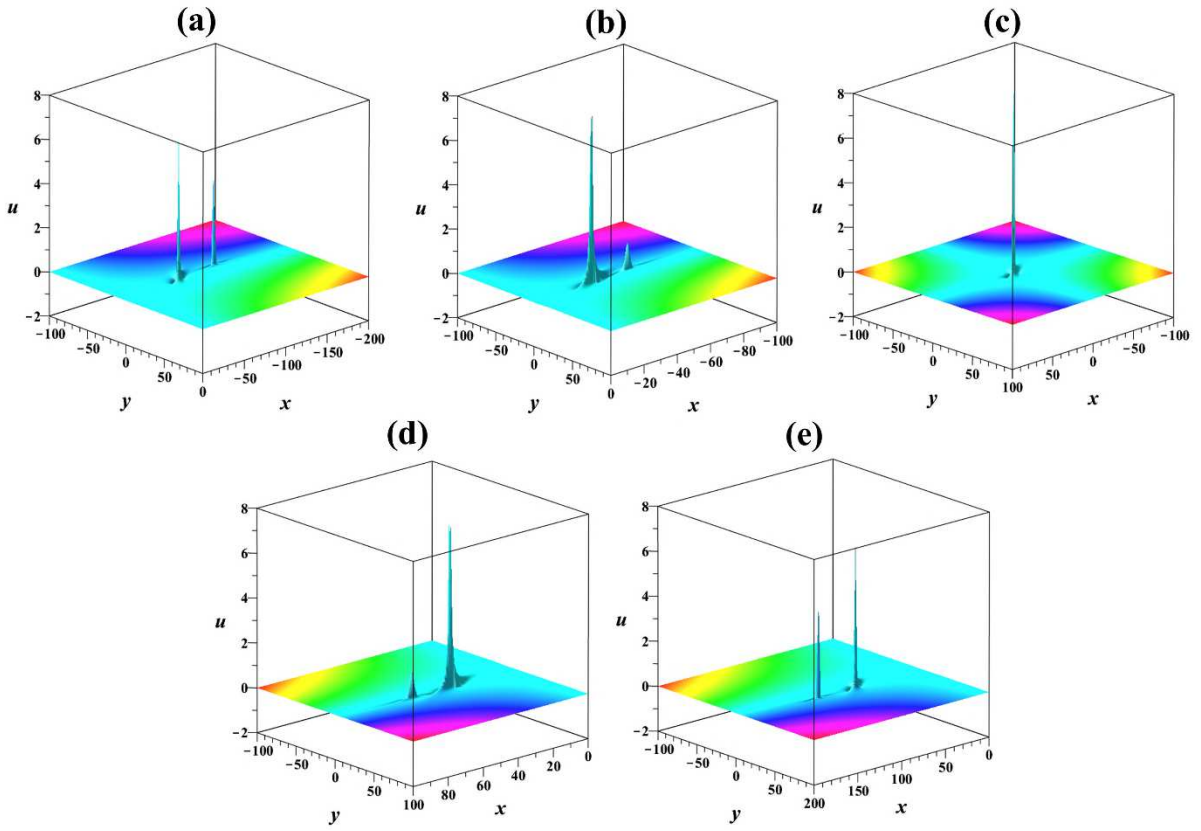

Figure 13. Time evolution 3D plots of the interaction solutions between two lump soliton solutions given by Eq. (51) at (a) $t = -50$, (b) $t = -25$, (c) $t = 0$, (d) $t = 25$, and (e) $t = 50$ under constraint parameters as $m_1 = m_2^* = -1 + I$, $m_3 = m_4^* = -1 + 10I$, $\alpha = 1$, $\beta = 1$, $\gamma = 1$, and $\delta = 1$.